

1 **Deglacial records of terrigenous organic matter accumulation off the**
2 **Yukon and Amur rivers based on lignin phenols and long-chain *n*-**
3 **alkanes**

4 Mengli Cao¹, Jens Hefter¹, Ralf Tiedemann^{1,2}, Lester Lembke-Jene¹, Vera D. Meyer³,
5 Gesine Mollenhauer^{1,2,3}

6 ¹Alfred-Wegener-Institut, Helmholtz-Zentrum für Polar-und Meeresforschung (AWI),
7 27570 Bremerhaven, Germany.

8 ²Department of Geosciences, University of Bremen, 28359 Bremen, Germany.

9 ³MARUM-Center for Marine Environmental Sciences, University of Bremen, 28359
10 Bremen, Germany.

11 Corresponding author:

12 Mengli Cao, mengli.cao@awi.de

13 Gesine Mollenhauer, gesine.mollenhauer@awi.de

Abstract:

14 Arctic warming and sea level change will lead to widespread permafrost thaw
15 and subsequent mobilization. Sedimentary records of past warming events during the
16 last glacial–interglacial transition can be used to study the conditions under which
17 permafrost mobilization occurs, and which changes in vegetation on land are
18 associated with such warming. The Amur and Yukon rivers discharging into the
19 Okhotsk and Bering Seas, respectively, drain catchments that have been, or remain
20 until today, covered by permafrost. Here we study two marine sediment cores
21 recovered off the mouths of these rivers. We use lignin phenols as biomarkers, which
22 are excellently suited for the reconstruction of terrestrial higher plant vegetation, and
23 compare them with previously published lipid biomarker data.

24 We find that in the Yukon Basin, vegetation change and wetland expansion began
25 already in the early deglaciation (ED, 14.6–19 ka BP). This timing is different from
26 observed changes in the Okhotsk Sea reflecting input from the Amur Basin, where
27 wetland expansion and vegetation change occurred later in the Preboreal (PB). In the
28 two basins, angiosperm contribution and wetland extent all reached maxima during
29 the PB, both decreasing and stabilizing after the PB. The permafrost of the Amur
30 Basin began to become remobilized in the PB. Retreat of sea-ice coupled with
31 increased sea-surface temperatures in the Bering Sea during the ED might have
32 promoted early permafrost mobilization. In modern Arctic river systems, lignin and *n*-
33 alkanes are transported from land to the ocean via different pathways, i.e., surface
34 runoff vs. erosion of deeper deposits, respectively. However, accumulation rates of

35 lignin phenols and lipids are similar in our records, suggesting that under conditions
36 of rapid sea-level rise and shelf flooding, both types of terrestrial biomarkers are
37 delivered by the same transport pathway. This finding suggests that the fate of
38 terrigenous organic matter in the Arctic differs both on temporal and spatial scales.

1. Introduction

39 Climate warming caused by anthropogenic perturbation affects the Arctic more
40 strongly than other regions of the world. Warming climate induces environmental
41 changes that accelerate degradation of organic matter (OM) stored in permafrost and
42 promote greenhouse gas release (Strauss et al., 2013; Hugelius et al., 2014; Schuur et
43 al., 2015). Permafrost, or permanently frozen ground, is soil, sediment, or rock that
44 remains at or below 0 °C for at least two consecutive years. It occurs both on land and
45 on the continental shelves offshore, and underlies about 22 % of the Earth's land
46 surface (Brown et al., 2002; Wild et al., 2022). Permafrost regions around the world
47 store twice as much carbon as is contained in the atmosphere at present (Hugelius et
48 al., 2014; Friedlingstein et al., 2020). Across the northern circum-polar permafrost
49 regions, the surface permafrost carbon pool (0–3 m depth) amounts to 1035 ± 150 Pg
50 (Hugelius et al., 2014). Warming climate may lead to increased mobilization of this
51 carbon pool, while it also affects the type and extent of the vegetation cover, which in
52 turn influences permafrost stability.

53 During the most recent interval of rapid global warming from the end of the Last
54 Glacial Maximum (LGM) to the early Holocene (~19–11 ka BP), the climate system
55 underwent large-scale change (Clark et al., 2012). Viau et al. (2008) found that the
56 summer temperatures in eastern Beringia (the non-glaciated region between the
57 Eurasian and the Laurentian ice sheet during the Late Pleistocene) during the LGM
58 were approximately 4°C lower than the present and increased rather rapidly toward
59 the Holocene. Sea-ice extent and distribution changed dramatically with consequences
60 for atmospheric moisture content (Ballantyne et al., 2013) and increased heat
61 transport from the oceans to the continental interiors (Lawrence et al., 2008). The
62 increase of precipitation inland as a result of sea ice retreating affects the stability of
63 permafrost in the Arctic (Vaks et al., 2020). Together with increasing air temperatures
64 during the deglaciation, sea-ice retreat may thus have led to rising ground
65 temperatures, active layer deepening and permafrost degradation.

66 Increased moisture due to sea ice retreat leads to heavier winter snowfall inland
67 (Liu et al., 2012; Park et al., 2013). Menard et al. (1998) reported that ground surface
68 temperature was higher where ground is covered by thick snow and shrubs and trees
69 than where it was covered by both thin snow and vegetation (moss and lichen).
70 During the last deglacial toward the Holocene, warming ground ice melted, causing
71 the land surface to collapse into space previously occupied by ice wedges, a process
72 called thermokarst. This led to the formation of thermokarst lakes and thermo-
73 erosional valleys as well as rivers, and also likely the release of carbon from thawed
74 deposits (Walter et al., 2006; Walter Anthony et al., 2014). During millennia following
75 the formation of thermokarst lakes, mosses and other plants grew in and around them,
76 which may in part have offset permafrost carbon release (Walter Anthony et al., 2014;
77 Schuur et al., 2015; Turetsky et al., 2020). Several studies suggested major deglacial
78 changes in the vegetation of permafrost-affected areas during the last deglaciation,
79 including the Lena River basin (Tesi et al., 2016), the Yukon Territory (Fritz et al.,
80 2012), the Amur River basin (Seki et al., 2012), and the Sakhalin peninsula and
81 Hokkaido (Igarashi and Zharov, 2011), the latter two bounding the Okhotsk sea to the
82 Northwest and North. Vegetation has a profound impact on distribution and thickness
83 of active layers, and permafrost in cold regions; for example, evidence exists that
84 permafrost temperature in the tundra is lower than in the boreal forest in northwestern
85 Canada (Smith et al., 1998), illustrating the strong effects of vegetation on permafrost
86 stability. Changes in vegetation should therefore be considered when investigating
87 permafrost stability in a changing climate.

88 Biomarker compositions, distributions, and contents in marine sediments can
89 help to elucidate the vegetation development in adjacent land areas (Winterfeld et al.,
90 2015, 2018; Keskitalo et al., 2017; Martens et al., 2019; Wu et al., 2022). Lignin is a
91 biopolymer exclusively biosynthesized by vascular plants. The relative abundance of
92 individual phenolic monomers varies between different plant types, and the different
93 phenols also differ in their stability towards degradation (Hedges and Mann, 1979;
94 Hedges et al., 1988; Lobbes et al., 2000; Feng et al., 2013; Wild et al., 2022). Ratios
95 between different phenolic monomers are thus sensitive indicators for vegetation type
96 and depositional history of OM originating from land plants (Hedges and Mann, 1979;
97 Hedges et al., 1988).

98 Previous studies found that the delivery of lignin from land to the ocean is
99 mainly controlled by surface discharge in modern Arctic river systems (Feng et al.,

100 2013) and has the potential to provide information on surface runoff processes and
101 wetland extent (Tesi et al., 2016; Feng et al., 2015). Long-chain *n*-alkanes (Alk) with
102 a strong predominance of the odd carbon number homologues, as well as even-
103 numbered long-chain *n*-alkanoic acids, derived from the epicuticular waxes of
104 vascular and aquatic plants (Eglinton and Hamilton, 1967). In contrast to lignin
105 phenols, sedimentary records of Alk, due to their recalcitrance, likely trace terrigenous
106 OM which has been mobilized from thawing permafrost deposits in modern Arctic
107 river systems (Feng et al., 2013) and may be transported into the marine sediment
108 primarily following coastal erosion during shelf flooding (Winterfeld et al., 2018).
109 Previous studies have reconstructed the mobilization of terrigenous OM from
110 degrading permafrost in the Okhotsk (Winterfeld et al., 2018) and Bering shelves
111 (Meyer et al., 2019) during the last deglaciation based on long-chain *n*-alkyl lipids
112 results. However, no records exist that combine lignin and Alk data to explore the
113 potentially different transport of terrestrial OM archived in Arctic marine sediments
114 during the last deglaciation.

115 Biomarker records can also be used to infer environmental conditions like sea-
116 surface temperatures (SSTs) or sea-ice extent that influence heat and moisture
117 transport from the ocean to the continents. A commonly used proxy for the
118 reconstruction of SSTs is the TEX₈₆, which relies on the relative abundance of so-
119 called isoprenoid glycerol dialkyl glycerol tetraether lipids (GDGTs) with different
120 numbers of cyclopentyl moieties (Schouten et al., 2002). These compounds are
121 derived from the membranes of marine *Thaumarchaeota* and have been found to
122 record temperature conditions of their habitat. Sea-ice reconstructions rely on the
123 abundance of highly branched isoprenoids derived from diatoms adapted to life in
124 sea-ice (IP₂₅; Belt et al., 2007). Applying the TEX₈₆ temperature proxy, Meyer et al.
125 (2016) found that atmospheric teleconnections with the north Atlantic were a
126 widespread control on SST in the northwest Pacific and its marginal seas during the
127 past 15.5 ka. The TEX₈₆-derived SST implies that a widespread of northwest Pacific
128 SST to atmospheric teleconnections with north Atlantic climate decrease during the
129 early deglaciation, and summer insolation and CO₂ concentration in atmosphere were
130 important factor driving the SST evolution during this time (Meyer et al., 2016).
131 GDGTs can also be used to reconstruct terrigenous input to the ocean, when the
132 relative abundance of branched GDGTs derived mainly from soil bacteria and of
133 isoprenoid GDGTs is quantified by the branched and isoprenoid tetraether (BIT)

134 index (Hopmans et al., 2004). According to lignin phenols and the BIT index, Seki et
135 al. (2014a) found that terrestrial OM from the Amur River is a major source of OM in
136 the North Pacific Ocean at present and that terrestrial OM in surface sediments is
137 dominated by gymnosperms in the Okhotsk Sea.

138 In this study, we present downcore records of lignin phenols from the early
139 deglaciation to the Holocene obtained from sediment cores from off the Amur and
140 Yukon rivers draining permafrost affected by deglacial climate change. These sites in
141 the Okhotsk and Bering Seas, respectively, record conditions at two contrasting river-
142 dominated continental margins in the North Pacific area. We interpret the lignin
143 phenol records in the context of vegetation and wetland development and investigate
144 the temporal evolution of the different pathways of terrigenous OM export to the
145 ocean by comparing different types of terrigenous biomarker records, i.e., Alk from
146 published studies and new lignin phenol data as well as BIT index values. We further
147 investigate new and published biomarker-based reconstructions of SST, as well as
148 published biomarker-based sea-ice reconstructions to unravel the controls on
149 terrigenous OM transport to the ocean from thawing permafrost landscapes.

2. Study area

150 The Bering Sea is located north of the Pacific Ocean (Figure 1). The Yukon River is
151 the fourth largest river in North America in terms of annual discharge, and drains into
152 the Bering Sea (Holmes et al., 2012). The deglacial sediments from the Bering Sea
153 contain records both of sea-level rise-induced erosion of the vast Bering Shelf, and of
154 runoff from the Yukon River (Kennedy et al., 2010; Meyer et al., 2019). The Yukon
155 Basin was mostly unglaciated during the LGM, but had permafrost (Schirmer et al.,
156 2013). Although some permafrost in the Yukon Basin thawed during the last
157 deglaciation (Meyer et al., 2019; Wang et al., 2021), most of the basin is still covered
158 by permafrost today (Fig. 1). Arctic coastal erosion is rapid today, with average rates
159 of erosion at 0.5 m year^{-1} (Lantuit et al., 2012; Irrgang et al., 2022). Sea level rise will
160 lead to greater wave impact on arctic shorelines which increases the coastal erosion
161 (Lantuit et al., 2012). This suggests that during past times of rapid sea-level increase
162 like in the B/A and PB periods coastal erosion was more intense than it is today
163 (Lambeck et al., 2014; Fig. 2, b). Coastal erosion causes a large amount of terrigenous
164 OM to enter the ocean (Couture et al., 2018; Winterfeld et al., 2018), suggesting that
165 during past periods of sea-level rise, similar to today or even stronger erosive forces

166 were at play supplying vast amounts of terrigenous materials to marine sediments.
167 Pollen records indicate there were no significant changes in vegetation pattern from
168 the LGM to about 16 ka BP, but after about 16 ka BP, birch (one of the first trees to
169 develop after the glacier retreated) pollen became significantly more abundant from
170 western Alaska to the Mackenzie River (Bigelow, 2013). In the early Holocene,
171 significant *Populus-Salix* (cottonwood-willow) woodland development occurred in
172 interior Alaska and in the Yukon Territory (Bigelow, 2013), suggesting both
173 increasing summer temperature and moisture. Alder grows in a warmer and wetter
174 environment than birch, and it is a common genus in Yukon Holocene pollen records
175 (Schweger et al., 2011). Today the catchment of the Yukon River is covered by spruce
176 forest (20 %), grassland (40 %), shrubland (20 %), and open water and wetlands
177 associated with the lowland areas (8 %) (Amon et al., 2012).

178 The Okhotsk Sea, a semi-enclosed marginal sea located in the west of the North
179 Pacific, is known as the southernmost region of seasonal sea ice in the Northern
180 Hemisphere today (Fig. 1). The continental slope off Sakhalin Island in the Okhotsk
181 Sea receives runoff from the Amur river, the largest river catchment in East Asia. The
182 Amur is also one of the largest rivers in the world in terms of the annual total output
183 of dissolved OM and substantially influences the formation of seasonal sea ice
184 (Nakatsuka et al., 2004). The river originates in the western part of Northeast China
185 and flows east forming the border between China and Russia. The catchment of the
186 Amur transitioned from complete permafrost coverage during the LGM
187 (Vandenberghé et al., 2014) to almost entirely permafrost-free conditions at present.
188 The climate of the Amur Basin today is largely determined by continental patterns
189 from Asia, as the Asia monsoon influences the amount of precipitation from the
190 Pacific transported to this region during the summer. Previous studies found that
191 herbaceous plants were the predominant vegetation in the last glacial periods in the
192 Amur Basin, and were replaced by gymnosperms during the deglaciation and
193 Holocene (Bazarova et al., 2008; Seki et al., 2012). These authors concluded that the
194 variations of vegetation change agree well with climate changes in East Russia with
195 dry conditions in the last glacial followed by wetter climate in the deglaciation and
196 early Holocene (Seki et al., 2012). Now, the vegetation of the Amur Basin belongs
197 mostly to the Taiga zone, with larch as the most common species in the area. The
198 upper reaches of the Amur Basin belong to the coniferous continental taiga at present.

199 The central areas are dominated by mixed coniferous and broad-leaved forests and the
200 coniferous larch forests are the predominant vegetation in the lower Amur Basin.

3. Material and methods

3.1. Sampling and age control

201 Piston core SO202-18-3 (60.13° N, 179.44° W, water depth: 1111 m) and neighboring
202 Kasten core SO202-18-6 (60.13° N, 179.44° W, water depth: 1107 m) were recovered
203 from the northeastern continental slope of the Bering Sea in 2009 during R/V Sonne
204 cruise SO202-INOPEX (Gersonde, 2012). The two cores can be treated as one
205 composite record according to their ultrahigh-resolution micro-X-ray-fluorescence
206 data, sediment facies analysis of laminae and radiocarbon dating results (Kuehn et al.,
207 2014). It represents an apparently continuous sedimentary sequence dated back to the
208 Last Glacial (~25 ka BP) (Kuehn et al., 2014). Selected samples from core SO202-18-
209 6 ($n = 20$, 10–589 cm core depth, 6.23–12.65 ka BP) and from core SO202-18-3 ($n =$
210 29, 447–1423 cm core depth, 12.99–24.1 ka BP) with an average temporal resolution
211 of ~510 years were analyzed for lignin-derived phenol contents.

212 The 23.7 m-long piston core SO178-13-6 (52.73° N, 144.71° E) was collected
213 from the Sakhalin margin in the Okhotsk Sea during the expedition SO178-KOMEX
214 with R/V Sonne (Dullo et al., 2004) (Fig. 1) with the lowermost interval
215 corresponding to ~17.5 ka (Max et al., 2014). Selected samples ($n = 51$, 100–2340 cm
216 core depth, 1.11–17.27 ka BP) from core SO178-13-6 were analyzed for lignin-
217 derived phenol contents with an average temporal resolution of ~340 years.

218 Radiocarbon-based age models for the two cores are from Kuehn et al. (2014) for
219 core SO202-18-3/6 and Lembke-Jene et al. (2017) for core SO178-13-6. The time
220 interval covered by the records will be subdivided into five intervals, the early
221 deglaciation (ED; 19–14.6 ka BP), the B/A (14.6–12.9 ka BP), the Younger Dryas
222 (YD; 12.9–11.5 ka BP), the Pre-Boreal (PB, 11.5–9 ka BP) and the Holocene (<9 ka
223 BP).

3.2. Laboratory analyses

224 The extraction of lignin phenols was carried out based on the method of Goñi and
225 Montgomery (2000a) and as described in Sun et al. (2017). Dried samples were
226 oxidized with CuO (~500 mg) and ~50 mg ferrous ammonium sulfate in 12.5 ml 2N
227 NaOH under anoxic conditions. The oxidation was conducted with a CEM MARS5
228 microwave accelerated reaction system at 150 °C for 90 min. After oxidation, known

229 amounts of recovery standards (ethyl vanillin and trans-cinnamic acid) were added to
230 the oxidation products. The alkaline supernatant was acidified to pH 1 with 37 % HCl.
231 The reaction products were subsequently recovered by two successive extractions
232 with ethyl acetate. The combined ethyl acetate extracts were evaporated under a
233 stream of nitrogen, then re-dissolved in 400 μ l pyridine. Prior to injection into the gas
234 chromatograph-mass spectrometer (GC-MS), an aliquot (30 μ l) was derivatized with
235 30 μ l bis-trimethylsilyl-trifluoroacetamide (BSTFA) + 1 % trimethylchlorosilane
236 (TMCS) (60 $^{\circ}$ C, 30 min). An Agilent 6850 GC coupled to an Agilent 5975C VL MSD
237 quadrupole MS operating in electron impact ionization (70 eV) and full-scan (m/z 50–
238 600) mode was used for analysis. The source temperature of the MS was set to 230 $^{\circ}$ C
239 and the quadrupole to 150 $^{\circ}$ C. The GC was equipped with a DB-1 MS column (30 m
240 \times 0.25 mm i.d., film thickness 0.25 μ m). Helium was used as carrier gas at a constant
241 flow rate of 1.2 ml min⁻¹. Samples were injected in splitless mode in a split/splitless
242 injector (S/SL) held at 280 $^{\circ}$ C. The temperature of the GC-MS column was
243 programmed from 100 $^{\circ}$ C (initially held for 8 min.), ramped by 4 $^{\circ}$ C min⁻¹ to 220 $^{\circ}$ C,
244 then by 10 $^{\circ}$ C min⁻¹ to 300 $^{\circ}$ C with a final hold time of 5 min.

245 Eight lignin-derived phenols were analyzed in this study. They can be classified
246 into three groups according to their plant sources and structures:

- 247 1. Vanillyl phenols (V) consisting of vanillin (Vl), acetovanillone (Vn) and
248 vanillic acid (Vd).
- 249 2. Syringyl phenols (S), comprising syringaldehyde (Sl), acetosyringone (Sn)
250 and syringic acid (Sd).
- 251 3. Cinnamyl phenols (C) that include *p*-coumaric acid (*p*-Cd) and ferulic acid
252 (Fd).

253 Vanillyl phenols can be found in all vascular plants, syringyl phenols exist only
254 in angiosperms. Cinnamyl phenols are exclusively present in non-woody tissues of
255 vascular plants. Therefore, the S/V and C/V ratios can be used to distinguish lignin
256 between woody and non-woody tissues of angiosperms and gymnosperms (Hedges
257 and Mann, 1979) (Fig. 4). Since S and C phenols are more easily degraded than V
258 phenols during lignin degradation, these two ratios can also be impacted by the
259 degradation degree of lignin (Hedges et al., 1988; Otto and Simpson, 2006) (Fig. 4).
260 Microbial degradation of lignin increase the relative abundance of phenolic acids of V
261 and S phenols, the ratios of vanillic acid to vanillin (Ad/Al)_v and syringic acid to

262 syringaldehyde (Ad/Al)_s are commonly used to reconstruct the degradation degree of
263 lignin (Ertel and Hedges, 1985; Hedges et al., 1988; Otto and Simpson, 2006) (Fig. 4).

264 Besides, we also included some other oxidation products that do not necessarily
265 originate from lignin, such as 3,5-dihydroxybenzoic acid (3,5Bd) and para-
266 hydroxybenzenes (P) like *p*-hydroxybenzaldehyde (Pl), *p*-hydroxybenzophenone (Pn),
267 and *p*-hydroxybenzoic acid (Pd). Unlike lignin-derived phenols (V, S, and C), 3,5Bd
268 is absent in plant tissues, but most enriched in peat (Goñi et al., 2000b; Amon et al.,
269 2012). The 3,5Bd/V ratio can be used as a tracer for wetland extent and to determine
270 the degree of degradation for terrigenous OM (Fig. 4).

271 These compounds were identified based on retention time and mass spectra.
272 Quantification was achieved by peak areas of the respective compounds and using
273 individual 5-point response factor equations obtained from mixtures of commercially
274 available standards analyzed periodically. The yields of Pl, Vl and Sl were corrected
275 by the recovery rate of ethyl vanillin and the recovery rate of trans-cinnamic acid was
276 applied to correct the yield of other lignin-derived compounds and 3,5Bd (Goñi et al.,
277 2000a, b). The standard deviation was determined from repeated measurements of a
278 laboratory internal standard sediment extract ($n = 12$) and for the carbon-normalized
279 concentration of the sum of the 8 lignin phenols ($\Lambda 8$, mg 100mg⁻¹ OC) equals 0.31.

280 Mass accumulation rates (MAR) of vascular plant-derived lignin phenols were
281 calculated as follows:

$$282 \text{MAR} = \text{SR} \times \rho, \quad (\text{Eq. 1})$$

$$283 \text{MAR-lignin} = \text{MAR} \times \Sigma 8 \div 100 \quad (\text{Eq. 2})$$

284 where MAR is the mass accumulation rate in g cm⁻² a⁻¹, SR is the sedimentation
285 rate in cm a⁻¹, and ρ is the dry bulk density in g cm⁻³. MAR-lignin is the mass
286 accumulation rate of lignin (mg cm⁻² a⁻¹). $\Sigma 8$ represents the content of the 8 lignin
287 phenols in mg 10g⁻¹ dry sediment.

288 According to previous studies, the odd-numbered *n*-alkanes in the range of C₂₃ to
289 C₃₃ are almost exclusively terrigenous (Eglinton and Hamilton, 1967; Otto and
290 Simpson, 2005). Therefore, we can use the mid to long chain length (high molecular
291 weight, HMW) Alk to reflect the contribution of terrigenous OM. Lignin MARs were
292 compared to published MARs of HMW Alk from the Okhotsk Sea (Winterfeld et al.,
293 2018) and the Bering Sea (Meyer et al., 2019). The MARs of HMW Alk from the
294 Bering Sea were recalculated from the published data (Meyer et al., 2019) in order to

295 compare the results of the two sediment cores. The HMW Alk quantified for the
296 Bering and Okhotsk Sea sediment cores are C₂₃, C₂₅, C₂₇, C₂₉, C₃₁ and C₃₃ (Fig. 2).

297 Alkanes also have been shown to provide a second marker for wetland extent via
298 the Paq index (Ficken et al., 2000). It represents the relative proportion of mid-chain
299 length Alk (C₂₃ and C₂₅) to long-chain Alk (C₂₉ and C₃₁). The Paq ratios shown in our
300 manuscript have been published by others. The Paq ratio of SO202-18-3/6 core was
301 published by Meyer et al. (2019). The Paq ratio of SO178-13-6 core was published by
302 Winterfeld et al. (2018). We also cited the Paq ratio of the XP07-C9 core (Seki et al.,
303 2012), which was retrieved from the Okhotsk Sea (Fig. 1).

304 We further report here the relative abundances of isoprenoid GDGT lipids. These
305 data were obtained together with the same total lipid extracts that were used for Alk
306 data published by Meyer et al. (2019). The isoprenoid GDGTs were determined using
307 the methodology described in Meyer et al. (2016). In brief, the internal standard of
308 GDGTs (C₄₆-GDGT) was added to known amounts of dry sediment, and total lipid
309 extracts were obtained by ultrasonication with dichloromethane:methanol = 9:1
310 (vol/vol), 3 times. After extraction and saponification, neutral compounds (including
311 GDGTs) were recovered with *n*-hexane. Different compound classes were separated
312 by 1% deactivated SiO₂ column chromatography. Polar compounds (including
313 GDGTs) were eluted with methanol:dichloromethane = 1:1 (vol/vol). Afterward they
314 were dissolved in hexane:isopropanol = 99:1 (vol/vol) and filtered with a
315 polytetrafluoroethylene filter (0.45 μm pore size). Samples were brought to a
316 concentration of 2 μg μl⁻¹ prior to GDGT analysis. GDGTs were analyzed by high-
317 performance liquid chromatography and a single quadrupole mass spectrometer (see
318 Meyer et al. (2017) for more details).

319 The TEX₈₆ index can be used as a SST proxy (Schouten et al., 2002), with the
320 modified version TEX₈₆^L being applicable in settings where SST is below 15 °C (Kim
321 et al. 2010). The regional calibration of SST and TEX₈₆^L is based on Seki et al.
322 (2014b).

$$323 \text{TEX}_{86}^{\text{L}} = \log (\text{GDGT-2} / (\text{GDGT-1} + \text{GDGT-2} + \text{GDGT-3})) \quad (\text{Eq. 3})$$

$$324 \text{SST} = 27.2 \times \text{TEX}_{86}^{\text{L}} + 21.8 \quad (\text{Eq. 4})$$

325 The GDGT-1, GDGT-2, and GDGT-3 are isoprenoid tetraether lipids with 1, 2,
326 and 3 cyclopentane rings, which were detected by a single quadrupole mass
327 spectrometer. The MS detector was set for selected-ion monitoring of the following

328 (M + H)⁺ ions: m/z 1300.3 (GDGT-1), 1298.3 (GDGT-2), 1296.3 (GDGT-3) (Meyer
329 et al., 2016). SST is the sea surface temperature in °C.

330 The BIT index proxy is based on the abundance ratio of branched GDGTs to
331 isoprenoid GDGTs (Hopmans et al., 2004); higher BIT values suggest more
332 contributions from terrestrial soil OM (Weijers et al., 2006; Fig. 3). The BIT index is
333 calculated as $BIT = (GDGT-I + GDGT-II + GDGT-III) / (GDGT-I + GDGT-II +$
334 $GDGT-III + GDGT-IV)$. GDGT-I, GDGT-II, and GDGT-III refer to the concentration
335 of branched GDGT, GDGT-IV refers to the concentration of isoprenoid GDGT
336 (crenarchaeol). The MS detector was set for selected-ion monitoring of the following
337 (M + H)⁺ ions: m/z 1022 (GDGT-I), 1036 (GDGT-II), 1050 (GDGT-III), and 1292.3
338 (GDGT-IV) (Meyer et al., 2016).

4. Results

4.1. Lignin concentrations and MARs

339 Lignin phenol concentrations were 0.19–1.43 mg 100mg⁻¹ OC (Λ8) or 0.20–1.07 mg
340 10g⁻¹ sediment (Σ8) in the Bering Sea sediments and 0.32–1.29 mg 100mg⁻¹ OC or
341 0.40–2.16 mg 10g⁻¹ sediment in the Okhotsk Sea record. Overall, the MAR of lignin
342 is lower in the Bering Sea than in the Okhotsk Sea (Fig. 2c, d). During the ED, the
343 lignin MAR began to increase in the Bering Sea sediment and kept increasing until it
344 reached a maximum (17.70 μg cm⁻² a⁻¹) at the B/A-YD transition (Fig. 2c). After the
345 B/A, the lignin MAR started to decrease in the Bering Sea until the onset of the YD.
346 The lignin MAR in the Bering Sea reached a more pronounced but short maximum
347 (20.61 μg cm⁻² a⁻¹) at the YD-PB transition, followed by a decrease to the Holocene.
348 The lignin MAR in the Okhotsk Sea is more variable than in the Bering Sea record
349 (Fig. 2d). The lignin MAR shows an initial maximum in the B/A, but reaches a more
350 pronounced second peak (31.16 μg cm⁻² a⁻¹) in the early PB. Similar to the Bering Sea,
351 the lignin MAR decreased after about 11 ka BP and into the Holocene, however, the
352 lignin MAR in the Okhotsk Sea sediment featured a rather broad maximum between
353 B/A and early Holocene.

354 Deglacial changes in the MARs of HMW Alk have previously been reported for
355 the same cores (Meyer et al., 2019; Winterfeld et al., 2018). The MAR of lignin and
356 HMW Alk changed mostly synchronously in the Bering Sea, but in the Okhotsk Sea,
357 the increase in lignin MAR occurred later than in Alk MAR, and notably also later
358 than in the Bering Sea (Fig. 2c, d). Alk MAR in the Okhotsk Sea featured two similar

359 maxima in the B/A and during the YD-PB transition, while the lignin MAR maximum
360 in the B/A is less pronounced than that at the YD-PB transition. Lignin MAR are
361 more variable than Alk MARs between 10 and 7.8 ka BP.

4.2. Sea surface temperature in the Bering Sea (BIT and TEX₈₆^L)

362 Most BIT values in the Bering Sea are below the commonly assumed threshold value
363 of 0.3 (Fig. 3, Ic), above which SST reconstructions are potentially biased by
364 terrigenous isoGDGTs (Weijers et al., 2006). We are confident that in our study area,
365 marine-derived GDGTs dominate over terrigenous GDGTs, suggesting that TEX₈₆^L is
366 not biased by terrigenous input.

367 The SST estimates derived from the TEX₈₆^L index are shown in Fig. 3, Ic. The
368 deglacial evolution of the TEX₈₆^L-derived SST shows an overall warming, from ~4.5
369 at 23.4 ka BP to 10.8 °C at 12.0 ka BP. The SST in the Bering Sea remained rather
370 constant during the LGM and the ED. The onset of the B/A is characterized by an
371 abrupt temperature increase of ~2 °C, followed by a decrease at the end of the B/A. At
372 the end of the YD, the SST abruptly increased by ~2 °C, while staying rather constant
373 from 11.5 ka BP to 10 ka BP. At the end of PB, the SST decreased slowly by 1°C
374 from 10.5 to 9.0 ka BP. During the Holocene, the SST ranged between 8.0 °C and
375 9.7 °C.

4.3. Lignin source and degradation indicators

376 Vegetation development can be assessed using the S/V (angiosperm vs. gymnosperm)
377 and C/V ratios (woody tissues vs. non-woody tissues) (Hedges and Mann, 1979). The
378 3,5Bd/V and Paq ratios can be used to indicate the change of wetland extent in the
379 study area (Goñi et al., 2000b; Amon et al., 2012). Similar to (Ad/Al)_s and (Ad/Al)_v
380 ratios, S/V, C/V, and 3,5Bd/V ratios are also affected by degradation processes (Ertel
381 and Hedges, 1985; Hedges et al., 1988; Otto and Simpson, 2006).

382 The S/V and C/V ratios yielded values of 0.36–0.86 and 0.11–0.46 in the Bering
383 Sea (Fig. 4, Ia, b), while slightly higher ratios of 0.41–0.92 and 0.19–0.70 were
384 obtained in the Okhotsk Sea (Fig. 4, IIa, b). The standard deviations for S/V and C/V
385 are 0.08 and 0.10, respectively. In the Bering Sea, the S/V ratios began to increase
386 from 18 ka BP and kept increasing until it reached a maximum in the transition of the
387 YD to the PB. The change of C/V values was not as obvious as S/V values, but it also
388 reached its maximum at YD-PB transition. Subsequently, S/V and C/V ratios
389 decreased during the Holocene and reached minima at the top of the core.

390 In the Okhotsk Sea, the S/V values increase slowly from the ED to PB, but the
391 C/V ratios do not display an obvious increase over the same time, except for a
392 maximum in C/V ratios around 15 ka BP. Minimum values were found in the ED and
393 values remained rather low before the YD-PB transition. After reaching maxima in
394 the PB, S/V and C/V ratios decreased during the Holocene, stabilizing at a higher
395 level than during the ED.

396 In the Bering Sea, the 3,5Bd/V ratio ranged from 0.09 to 0.20 (Fig. 4, Id)
397 (standard deviation: 0.02). From the end of LGM to the YD, the 3,5Bd/V ratio
398 decreased slowly, but began to increase and reached a small local maximum at the
399 YD-PB transition. During the Holocene, the 3,5Bd/V ratio decreased again and
400 reached the lowest values near the top of the core.

401 The 3,5Bd/V ratios in the core from the Okhotsk Sea range from 0.10 to 0.23
402 (Fig. 4, IId) (standard deviation: 0.02). The values were rather uniform throughout the
403 record, with the exception of a maximum during the PB, and the ratio remained rather
404 stable afterwards.

405 The (Ad/Al)_s and (Ad/Al)_v ratios ranged from 0.19 to 0.80 (standard deviation:
406 0.24) and 0.51 to 1.04 (standard deviation: 0.26), respectively, in the Bering Sea (Fig.
407 4, Ie, f). Maxima in (Ad/Al)_s and (Ad/Al)_v were reached in the Holocene and YD. The
408 Ad/Al ratio in the Bering Sea showed low values during the PB and increased towards
409 the early Holocene, when highest values of Ad/Al were obtained.

410 In the Okhotsk Sea, the (Ad/Al)_s and (Ad/Al)_v ratios are overall similar and
411 range from 0.30 to 0.79 (standard deviation: 0.24) and from 0.22 to 0.89 (standard
412 deviation: 0.26), respectively (Fig 4, IIe, f). The (Ad/Al)_v ratio decreased slowly until
413 10.5 ka BP when the biomarker MARs reached maxima. All minima and maxima in
414 both indices occurred in the PB. Throughout the rest of the Holocene, Ad/Al values
415 remained rather constant.

5. Discussion

5.1. Terrigenous OM mobilization during the last deglaciation

416 Permafrost remobilization has a strong impact on local topography, vegetation, and
417 OM fate (Feng et al., 2013; Walter Anthony et al., 2014). We observed distinct MAR
418 peaks of terrigenous biomarkers in both sediment cores, but the temporal evolution of
419 MARs and the relative magnitude of change differ between the sites.

420 In the Bering Sea, lignin MAR began to increase at ~17.5 ka BP, which coincides
421 with the onset of sea level rise (Fig. 2). Wang et al. (2021) found that the Alaskan
422 mountain glaciers and Laurentide and Cordilleran ice sheets reached their maximum
423 extent from 20 ka BP to 16.5 ka BP, suggesting permafrost of the Yukon Basin may
424 not have begun to be remobilized during this time. The Yukon River discharge did not
425 increase until 16.5 ka BP (Wang et al., 2021), the terrigenous OM transported by
426 surface runoff thus may not have increased at ~17.5 ka BP. Keskitalo et al. (2017)
427 found that the OM flux accumulated on the East Siberian Shelf during the PB-
428 Holocene transition was high and these OM were characterized by high S/V (0.28–
429 0.90, mean value is 0.50) and C/V values (0.19–0.60, mean value is 0.35) (Fig. 5).
430 These authors suggested the Ice Complex Deposit (ICD) as a significant source of
431 OM in the East Siberian Sea during this time. Previous studies indicated that ICD
432 samples yield relatively high S/V and C/V ratios ranging from 0.47 to 1.01, and from
433 0.03 to 0.82, indicating the OM is likely to stem from grass-like material typical of
434 tundra or steppe biome (Schirrmeister et al., 2013; Tesi et al., 2014; Winterfeld et al.,
435 2015). The S/V (0.50–0.75, mean value is 0.62) and C/V (0.22–0.36, mean value is
436 0.28) values of the Bering Sea sediment core from 24 ka BP to 17.5 ka BP are high
437 (Fig. 4, I), which may indicate that this terrestrial OM is likewise derived from the
438 ICD. The organic-rich ICD on the coasts of the Bering Sea might have been inundated
439 or eroded by rising sea level in the ED, which may contribute to the lignin MAR in
440 the Bering Sea at ~17.5 ka BP.

441 HMW Alk accumulation in the Bering Shelf started to increase around 16.5 ka
442 BP (Fig. 2), which coincides with the beginning retreat of Alaskan glaciers (Dyke,
443 2004). The glacial meltwaters drained through the Yukon River and enhanced fluvial
444 discharge to the Bering Sea (Wang et al., 2021). The ICD in Alaska and Beringia
445 might have started to be remobilized at ~16.5 ka BP (Meyer et al., 2019; Wang et al.,
446 2021), subsequently enhancing the MAR of ICD-derived OM off the Bering Shelf.
447 Thus, the increased S/V, C/V, and Paq values near 17.5 ka BP (Fig. 4, Ia–c) lend
448 support to the notion that permafrost of the Yukon Basin may have begun to be
449 remobilized in the ED.

450 Retreat of sea ice will increase the SST, and open waters increase the moisture
451 content of the atmosphere, so the transport of heat from the ocean via atmospheric
452 pathways to continental interiors increases (Ballantyne et al., 2013; Vaks et al., 2020).
453 Praetorius et al. (2015) found that SST warming commenced around 16.5 ka BP (core

454 85JC, Fig. 3, If) in the northern Gulf of Alaska, and Méheust et al. (2018) observed
455 rising SST of the northeast Pacific by ~ 1.5 °C near 16 ka BP (core SO202-27-6, Fig. 3,
456 Ie) which agrees with our $\text{TEX}_{86}^{\text{L}}$ -SST record (core SO202-18-3/6, Fig. 3, Ic). The
457 same authors reconstructed sea-ice extent based on the IP_{25} proxy to decrease from
458 around 16 ka BP in the Northeast Pacific (Fig. 3, Ie). Jones et al. (2020) reported that
459 the sea ice in the Bering Sea is highly sensitive to small changes in winter insolation
460 and atmospheric CO_2 . Further evidence for regional climate warming in the hinterland
461 of Alaska is provided by the Brooks Range glacial melting during a time of
462 widespread cooling in the Northern Hemisphere (Dyke, 2004; Wang et al., 2021).
463 Combined evidence from SST and sea-ice reconstructions as well as records of glacial
464 melting thus suggest that the permafrost of the Yukon Basin may have begun to be
465 remobilized at ~ 16 ka BP.

466 In the B/A, all biomarker fluxes increased and reached short maxima (Fig. 2c, d).
467 The rate of sea level rise also reached a maximum since the LGM. If Alk had been
468 transported to the ocean primarily through coastal erosion, as is the case with the
469 modern Arctic river transport systems (Feng et al., 2013), then Alk MAR would have
470 been at its maximum, but it was not. Warming may have caused widespread
471 permafrost thaw in the Yukon Basin in the B/A. At this time, SST increased, sea-ice
472 cover decreased (Méheust et al., 2018), and an increase in river discharge was
473 reconstructed (Wang et al., 2021), which may have fostered diatom bloom events
474 (Kuehn et al., 2014; Fig. 2).

475 Increased S/V, and decreased $(\text{Ad/Al})_{\text{s,v}}$ in the B/A, suggesting that the OM
476 deposited in the Bering Sea during the B/A may have been derived from ICD. Similar
477 to our findings, Martens et al. (2019) found relatively high lignin fluxes in the
478 Chukchi Sea during the B/A (Fig. 2e) and showed that lignin deposited during this
479 period was poorly degraded. The authors interpreted this degradation state as
480 permafrost OM from ICD being the dominant source. The relative contribution of
481 ICD and the main pathway of transportation (abrupt thaw or gradual thaw on land)
482 cannot be deduced from our data alone. Further analyses may reveal possible ICD
483 contributions to lignin exported to the marine realm during this interval.

484 During the YD-PB transition, the Northern Hemisphere experienced an abrupt
485 temperature increase, the maxima of biomarker MAR (Fig. 2c) indicate that the
486 permafrost remobilization in the Yukon Basin reached a peak at this time. The Yukon
487 River discharge increased during the PB (Wang et al., 2021) which can also promote

488 lignin flux. Evidence for widespread permafrost decomposition and wetland
489 expansion at the same time has been reported from the Bering Sea (Meyer et al.,
490 2019), the Siberian-Arctic (Tesi et al., 2016; Martens et al., 2020), and eastern
491 Beringia (Kaufman et al., 2015). Bering Sea sediments deposited during the time
492 intervals of lignin MAR peaks were laminated (Fig. 2c), indicating increased export
493 productivity and terrigenous OM supply may have promoted anoxic conditions during
494 the YD-PB transition (Kuehn et al., 2014).

495 The rate of sea level change was lower during the PB than that in the B/A, but
496 the MARs of Alk and lignin reached maxima, and the discharge of the Yukon also
497 increased from the B/A to the PB. Therefore, both coastal erosion and surface runoff
498 may affect the transport of Alk and lignin from land to ocean in the Yukon Basin
499 during the last deglaciation.

500 Different from the Bering Sea records, lignin MAR did not yet increase in the
501 Okhotsk Sea during the ED (Fig. 2d), except for a short peak at the transition from the
502 ED to the B/A. The discharge of the Amur River was low, but the MAR of lignin
503 increased at the transition from the ED to the B/A when the rate of sea level change
504 was rapid. At the same time, the Alk MAR did not change significantly (Fig. 2). This
505 suggests that both lignin MARs in Okhotsk Sea sediment are affected by coastal
506 erosion during the last deglaciation.

507 SSTs were higher in the Northeast Pacific and the Bering Sea than in the
508 Northwest Pacific and Okhotsk Sea during the ED, and the IP₂₅ value was relatively
509 high in the Okhotsk Sea (Fig. 3, IIc), indicating the sea ice of the Okhotsk Sea did not
510 begin to retreat in the ED (Lo et al., 2018). Caissie et al. (2010) found that the first
511 detectable concentration of alkenones in the Bering Sea sediment at 16.7 ka BP
512 occurred earlier than in the Okhotsk Sea, although the Bering Sea is located further
513 north than the Okhotsk Sea. As a result of prevailing sea-ice cover, the permafrost of
514 the Amur Basin may have remained stable in the ED (Vaks et al., 2013, 2020;
515 Winterfeld et al., 2018; Meyer et al., 2019).

516 The rate of sea-level change reached a peak during MWP-1A (Fig. 2d) which
517 likely also caused an increase in the rate of coastal erosion. Thus, the increased
518 biomarker MAR during the B/A (Fig. 2) may be attributed largely to coastal erosion.
519 This suggests that both types of biomarkers are supplied via the same erosive process
520 during the B/A, in contrast to findings from the modern-day Arctic.

521 From the YD to the PB, the Northern Hemisphere experienced an abrupt
522 temperature increase and the SST of the North Pacific increased significantly (Max et
523 al., 2012; Riethdorf et al., 2013; Méheust et al., 2016, 2018; Meyer et al., 2016, 2017).
524 All biomarker MARs in the Okhotsk Sea increased and reached maxima in the YD-
525 PB transition. The permafrost of the Amur Basin may have begun to be remobilized
526 coevally with previously reported periods of stalagmite growth starting after the PB in
527 the south of Siberia, which indicates the decay of permafrost and opening of water
528 conduits into the caves (Vaks et al. 2013, 2020). A pronounced lignin flux maximum
529 occurred during MWP-1B, coinciding with a period of enhanced discharge from the
530 Amur River. This implies that hinterland permafrost thawing played a more important
531 role in the land-ocean OM transport during the later deglaciation, which may have had
532 an impact on the oxygen content and nutrient concentration in the Okhotsk Sea
533 Intermediate Water in the MWP-1B (Lembke-Jene et al., 2017).

534 MARs decrease drastically after maxima in both the Okhotsk and Bering Seas
535 (Fig. 2c, d). The Amur Basin was completely covered with permafrost during the
536 LGM (Vandenberghé et al., 2014) and almost all of the permafrost was lost until today
537 as a result of permafrost mobilization during the last deglaciation. Thus, the
538 contribution of permafrost OM from the Amur Basin to the marine sediment began to
539 decrease in the early Holocene in agreement with the results of Seki et al. (2012).

540 In summary, the permafrost of the Amur Basin began to be remobilized in the PB
541 later than in the Yukon Basin. We suggest that this was caused by decreased sea ice or
542 increased SST in the Bering Sea during the ED, while the Okhotsk Sea remained ice-
543 covered. We found that during the last deglaciation, lignin and Alk were supplied
544 from land to the ocean via the same combined processes in the Yukon and Amur
545 Basins, including surface runoff and coastal erosion.

5.2. Vegetation changes in the two river basins

5.2.1. Yukon River Basin

546 As the climate warmed during the transition from the LGM to the ED, moisture
547 increased and an increasing number of thermokarst lakes developed in Alaska,
548 especially after about 16–14 ka BP (Bigelow, 2013; Walter et al., 2007). We observe
549 an increase in S/V ratios from the ED to the B/A, indicating increasing contributions
550 of angiosperms around this time, extending into the B/A (Fig. 4, 1a). The S/V and C/V
551 ratios are also influenced by the degradation of lignin, with increasing ratios
552 suggesting a lower degradation state (Hedges et al., 1988; Otto and Simpson, 2006),

553 but there is no parallel decrease in the more commonly used degradation indicator, i.e.,
554 the Ad/Al ratios, at the same time (Fig. 4, Ie, f). As the permafrost had begun to be
555 remobilized in the Yukon Basin during the ED, the S/V suggests that the cover of
556 angiosperms in this basin increased.

557 During the transition of ED-B/A, the rate of sea level change was rapid, implying
558 that the distance of our study site to the river mouth must have changed. The degree
559 of OM degradation, however, did not change significantly at the same time (Fig. 4, e,
560 f). Reports that the degradation degree of Lena River-derived OM and surface
561 sediments of Buor Khaya Bay are similar (Winterfeld et al., 2015) suggest that the
562 oxidative degradation of lignin occurred mainly on land, in agreement with our results.
563 We thus posit that transport within the ocean that might have increased in distance and
564 duration in response to the sea level change may only have a limited impact on OM
565 degradation in the Bering Sea. The S/V and C/V can thus be regarded to mainly
566 reflect vegetation development in the transition of ED-B/A. Anderson et al. (2003)
567 also found birch pollen becoming significantly more prevalent after about 16 ka BP
568 from western Alaska to the Mackenzie River, suggesting that these regions were
569 characterized by glacier retreating and more favorable climatic conditions. Coevally,
570 the Paq index (Fig. 4, Ic) shows an increase, indicating wetland expansion.

571 There is evidence that herb-dominated tundra was replaced by *Betula-Salix*
572 (birch-willow) shrub tundra around Trout Lake (the northern Yukon) during the B/A
573 (Fritz et al., 2012) as the climate warmed and became more humid than during the ED.
574 In line with these observations, our C/V ratios indicate that the contribution of non-
575 woody plant tissues was lower in the B/A than in the ED (Fig. 4, Ib).

576 After the B/A, the summer temperatures during the YD dropped by ~1.5 °C
577 (Fritz et al., 2012), thus cold-adapted non-arboreal plants briefly increased in
578 abundance (Fritz et al., 2012). The S/V ratios indicate that the non-woody angiosperm
579 plants' contribution reached a maximum in the Yukon Basin during the YD-PB
580 transition (Fig. 4, Ia). The MARs of biomarkers in the Bering Sea also reached
581 maxima during this transition (Fig. 2, c). Since the opening of the Bering Strait (~11
582 ka BP, Jakobsson et al., 2017), a trend of increase in *Betula* (birch) was observed in
583 eastern Beringia (Fritz et al., 2012; Kaufman et al., 2015) which indicates a
584 progressively more maritime climate developing in response to changes in the marine
585 environment (Igarashi and Zharov, 2011). Vegetation development and permafrost
586 remobilization both contribute to the biomarker MARs (Fig. 2, c). The BIT values

587 higher than 0.3 from 13 ka BP to 10.5 ka BP (Fig. 3, 1c) further support this
588 interpretation while at the same time indicating that in these intervals, TEX_{86}^L cannot
589 be used to reflect the sea surface temperature change during this interval. Additionally,
590 the intensification of oxygen minimum zones in the Bering Sea during the B/A (Fig.
591 2c) may be related to the increase in surface runoff (freshwater and OM fluxes; Kuehn
592 et al., 2014).

593 Since vegetation responds to changes in both temperature and moisture,
594 significant *Populus/Salix* (cottonwood/willow) woodland development occurred in
595 interior Alaska and the Yukon Territory during the early Holocene (Anderson et al.,
596 2003). However, the expansion of these angiosperm plants is not reflected in our S/V
597 record (Fig. 4, 1a), the interpretation of S/V ratios may be complicated by the
598 influence of degradation processes during the early Holocene. Pollen assemblages
599 from northern Siberian soils have shown that woody plants occurred only after the
600 onset of the Holocene (Binney et al., 2009), which agrees with a decrease in the C/V
601 ratios since the early PB into the early Holocene (Fig. 4, 1b).

602 We compare our S/V and C/V ratios with published values from sediment cores,
603 surface sediments and suspended materials in the Arctic and subarctic (Fig. 5). Such
604 plots can help to identify the main types of plant tissues the lignin phenols are derived
605 from, and enable the detection of potential degradation effects.

606 The S/V and C/V ratios from our Bering Sea core compare favorably with those
607 from a core recovered from the Chukchi shelf covering parts of the B/A and the YD as
608 well as the late Holocene (Martens et al., 2019) (Fig. 5). This may suggest that a
609 similar type of vegetation prevailed across much of Beringia. After the opening of the
610 Bering Strait, Pacific waters flowed into the Chukchi Sea, and it is conceivable that
611 the terrestrial material transported to the Bering Sea by the Yukon River may have
612 been in part transported into the Chukchi Sea. The top of our core dates to the early
613 Holocene, a period that was characterized by more widespread broad-leaf angiosperm
614 vegetation than today, which might explain the offset between our early Holocene S/V
615 and C/V ratios and those reported for Yukon River surface sediment (S/V: 0.28, C/V:
616 0.14) (Feng et al., 2015) and dissolved organic carbon in the Yukon (S/V: 0.47, C/V:
617 0.14) (Amon et al., 2012) at present. Degradation of lignin in sediments may explain
618 some of the discrepancies between sediment data and S/V and C/V ratios reported
619 from suspended materials collected in the modern Lena River (Fig. 5). As the Amur
620 River catchment is dominated by gymnosperms at present (Seki et al. 2014a), the S/V

621 ratios of the Amur River and Okhotsk Sea surface sediments (Seki et al., 2014a) are
622 lower than in the Bering Sea core (Fig. 5).

623 The highest values of the 3,5Bd/V ratio correlate with the enhanced degradation
624 of lignin phenols around 17.5 ka BP (Fig. 4, Id). This suggests that degraded OM is
625 the dominant source of the lignin phenols at this time, in agreement with previous
626 studies (Meyer et al., 2016, 2019). Global melt water pulses according to Lambeck et
627 al. (2014) occurred during the following periods: MWP-1A from 14.6 to 14.0 ka BP
628 and MWP-1B from 11.5 to 10.5 ka BP. The 3,5Bd/V and (Ad/Al)_s ratios decreased
629 slowly from the ED to the MWP-1A, which indicates that the change in 3,5Bd/V
630 values from the LGM to the early B/A reflects a variable degree of OM degradation,
631 rather than expansion of wetlands or peatlands. The 3,5Bd/V also featured a short
632 maximum during the late YD and early PB when the 3,5Bd/V signal is likely
633 dominantly ascribed to increases in wetland or peatland sources, as there is no parallel
634 maximum in Ad/Al ratios (Fig. 4, Id, e, f).

635 This pattern of 3,5 Bd/V change is not in agreement with the Paq ratio
636 determined for the same core earlier (Meyer et al., 2019), although both proxies may
637 reflect wetland expansion (Goñi et al., 2000b; Amon et al., 2012). The temporal
638 evolution of Paq is similar to that of S/V and C/V, where Paq began to increase in the
639 ED and reached its maximum in the YD-PB transition (Fig. 4, Ic), indicating that the
640 proxies are influenced to some extent by degradation.

641 The Ad/Al ratios decreased when the biomarker MAR peaked during MWP-1B
642 (Fig. 4, IIe, f) which may correspond to better preservation during rapid burial, or
643 higher contribution of ICD OM and fresh angiosperm debris. This better preservation,
644 is in agreement with previous studies (Anderson et al., 2003; Meyer et al., 2019).
645 Kuehn et al. (2014) found that increases in biological export production and
646 remineralization of OM in the Bering Sea during the B/A and PB reduced oxygen
647 concentration to below 0.1 ml L⁻¹ and caused the occurrence of laminated sediments
648 (Fig. 2c). This anoxic condition in the Bering Sea during the B/A and PB also slowed
649 down rates of OM decomposition and increased the accumulation of OM.

650 In summary, our data together with published evidence indicate that in the Yukon
651 Basin, vegetation change and wetland expansion began in the ED. Angiosperm plant
652 contribution and wetland extent all reached their maxima during the PB, both
653 decreasing and stabilizing at lower levels after the PB. During the PB, terrigenous

654 OM appeared least degraded, suggesting rapid supply and burial of rather well-
655 preserved terrigenous OM.

5.1.2. Amur River Basin

656 The lowest contribution of non-woody angiosperms as indicated by low S/V and C/V
657 ratios occurred at 16.6 ka BP (Fig. 4, IIa, b). Subsequently, both ratios increased and
658 reached maxima during the PB, suggesting the expansion of angiosperms and non-
659 woody tissues contributing substantially to lignin. After the PB, the S/V decreased
660 rapidly and remained stable during the Holocene, while the C/V ratio showed a
661 second maximum at 9.2 ka BP suggesting an increasing contribution of non-woody
662 angiosperms in the PB (Fig. 4, IIa, b). In agreement with our data, published lipid
663 records provide evidence that the vegetation in the Amur Basin did not change
664 significantly in the ED (Seki et al., 2012). Winterfeld et al. (2018) found a general
665 synchronicity of Amur River discharge and the northward extent of monsoon
666 precipitation in the early Holocene. Climate warming associated with high moisture
667 supply allowed the expansion of birch-alder forests in the Amur Basin in the PB
668 (Bazarova et al., 2008; Igarashi and Zharov, 2011).

669 C/V and S/V ratios indicate that the contribution of non-woody gymnosperm
670 tissue was higher in the early than in the later deglaciation (Fig. 6), similar to what has
671 been reported from East Siberian Shelf records (Keskitalo et al., 2017). The YD caused
672 only minor vegetation changes in the East Asian hinterland (Igarashi and Zharov,
673 2011). Our lignin records for this period are in agreement with previous studies that
674 indicated that the Lower Amur River basin mainly featured shrub birch-alder forests
675 and rare *Pinus* (Bazarova et al., 2008; Seki et al., 2012).

676 Non-woody angiosperm plant contributions to the Okhotsk Sea sediment
677 strongly increased during the PB (Fig. 4, IIa, b), when the summer insolation and
678 regional temperatures reached the highest values since the LGM. Significant
679 vegetation changes in the Amur Basin thus started in the PB period, temporally offset
680 from the Yukon Basin, and the contribution of angiosperms from 14.6 ka BP to 9 ka
681 BP appears to be higher than during the ED (Fig. 6). Bazarova et al. (2008) reported
682 based on pollen analyses that a turning point in vegetation development in the Amur
683 Basin occurred at a boundary of 10 ka BP. The Middle Amur depression registered the
684 first appearance of broad-leaved species of pollen and a prevalence of spores over
685 arboreal pollen at that time (Bazarova et al., 2008). The C/V ratio did not decrease as
686 rapidly as the S/V ratio after the peak and showed a second maximum at ~9 ka BP.

687 Some pollen of *Picea* (such as *P. glauca* and *P. mariana*) yield exceptionally high
688 amounts of cinnamyl phenols (Hu et al., 1999), which may have affected the C/V ratio
689 as the end member of woody/non-woody tissues. An et al. (2000) concluded that lakes
690 were deepest and most extensive around 10 ka BP in northeastern China (the upper
691 Amur basin), and 3,5Bd/V and Paq values reached maxima at the same time (Fig. 4,
692 IId, c) suggesting wetland extent peaked during the PB. Therefore, wetland plants that
693 have broad leaves, such as sedges, may also have a positive influence on the C/V ratio.

694 The S/V and C/V data from the Holocene part of our core do not agree with
695 published values for the Okhotsk Sea and Amur River surface sediments (Fig. 6).
696 During the past 250 years, vegetation was marked by significant rises of
697 gymnosperms, such as pines, combined with the reduction in the swamp area and a
698 large increase in fire activity (Yu et al., 2017), likely resulting in higher contributions
699 of gymnosperm to the surface sediment while these changes are not resolved in the
700 samples analyzed for our record.

701 The 3,5Bd/V and Paq ratios of the Okhotsk Sea both display relatively high
702 values during the PB (Fig. 4, IId, c). Seki et al. (2012) found high Paq values during
703 the PB in a nearby sediment core XP07-C9, and the values in their core were higher
704 than in ours (Fig. 4, IIc). Spores of *Sphagnum* show a distinct peak during the PB
705 (Morley et al., 1991), reflecting an expansion of mesic and boggy habitats. Our
706 records together with published evidence thus suggest that permafrost destabilization
707 and wetland expansion in the Amur Basin occurred only at the beginning of the PB,
708 while those processes were initiated much earlier in the Yukon basin.

709 The Ad/Al values were decreasing until 10.5 ka BP and reached minima during
710 the PB (Fig. 4e, f), indicating that low temperatures on land on the one hand, and
711 rapid burial in marine sediments during shelf flooding and coastal erosion during
712 MWP-1B on the other hand, contributed to the Ad/Al signals. The 1 ka averages of
713 the S/V, C/V ratios show similar minima as the Ad/Al ratios from the ED to the PB
714 (Fig. 4II), suggesting that degradation processes exert a strong control on the S/V and
715 C/V ratios during a time when vegetation did not change in the Amur Basin. In the
716 course of climate amelioration from around 11.6 ka BP (Tarasov et al, 2009), the rates
717 of vegetation development, wetland expansion and Amur River discharge (Fig. 2f) all
718 displayed maxima in the PB. Generally, higher Ad/Al values in the later part of the PB
719 suggest that fluvial runoff supplied more degraded lignin. Aerobic degradation of OM
720 in soils by fungi has also been shown to increase Ad/Al values (Goñi et al., 1993).

721 Since the oxidative degradation occurred mainly on land (Winterfeld et al., 2015), and
722 lateral transport is likely short, this increased degradation is unlikely to occur in the
723 ocean. The Okhotsk Sea shelf is narrower than the Bering Shelf and Siberian shelves,
724 the lateral shelf transport times (i.e., the cumulative time a particle spends in
725 sedimentation-resuspension cycles) of the Okhotsk shelf are therefore likely to be
726 much shorter than what has been reported for the Laptev Shelf (Bröder et al., 2018),
727 further supporting our interpretation.

728 The rate of sea level change in the Bering Sea (Manley, 2002) is slower than the
729 global average rate (Lambeck et al., 2014). The effect of sea level change on the
730 degradation process of terrestrial OM in the Bering Sea is limited. We are not aware
731 of a published local reconstruction of sea level change for the Okhotsk Sea from 20 ka
732 BP to the present, but we suggest that, since the shelf of the Okhotsk Sea is narrower
733 than that of the Bering Sea, the effect of sea level change on the Okhotsk shelf may be
734 neglected. Pre-aged OM and young OM can be transported from land to the marine
735 sediments in a variety of ways, such as coastal erosion and surface runoff, but the
736 relative contribution of different carbon pools could not be quantified by lignin and
737 Alk fluxes or other parameters (S/V, C/V, 3,5Bd/V, Ad/Al, and Paq), as they appear to
738 be transported through the same pathways during the last deglaciation. Further
739 investigation using compound-specific radiocarbon analysis is needed to quantify the
740 contribution of different carbon pools in marine sediments.

741 In summary, our records indicate that in the Amur Basin vegetation change and
742 wetland expansion began during the PB and in the early Holocene, in agreement with
743 previous paleo-vegetation studies. This timing is different from observed changes in
744 the Yukon Basin. However, similar to the Yukon Basin, the wetland extent and non-
745 woody angiosperm contribution were reduced and stabilized after the PB in the Amur
746 Basin. The increased vegetation and wetland indices, as well as increased degradation
747 of lignin in the Okhotsk Sea sediment at the end of the PB, may be related to changes
748 in the source of OM (shelf and coastal erosion vs. river transported material).

Conclusions:

749 By analyzing mass accumulation rates of terrigenous biomarkers in sediments from
750 the Bering and Okhotsk Seas, we provide the first downcore records of lignin from
751 the Yukon and Amur Basins covering the early deglaciation to the Holocene. We find
752 that vegetation changed earlier in the Yukon than in the Amur Basin. Although S/V,
753 C/V and 3,5Bd/V ratios can reflect vegetation change and wetland development, the

754 degradation state of lignin strongly overprints these proxy signals and should be
755 considered as a function of temperature, transport distance and burial rate. Similar to
756 changes in vegetation, we observe that degradation and remobilization of permafrost
757 of the Yukon Basin also occurred earlier than in the Amur Basin. Sea-ice extent and
758 SSTs of adjacent ocean areas might have had a strong influence on the timing of
759 hinterland permafrost mobilization. Our study reveals that lignin transported by
760 surface runoff may account for significant proportions of lignin during inland
761 warming, but the export of lignin and lipids do not always occur via different
762 pathways, as both biomarker groups can be contributed from rapidly eroding deep
763 deposits during phases of rapid permafrost thaw. In contrast to modern day evidence
764 suggesting different pathways for lipid and lignin biomarker transport, our records
765 imply that during glacial peaks of permafrost decomposition, lipids and lignin might
766 have been delivered to the ocean by identical processes, i.e., runoff and erosion.

767 **Authors' contributions**

768 MC measured and compiled lignin data, and wrote the manuscript with the help of all
769 co-authors. JH was responsible for all biomarker analyses. LLJ and RT provided
770 samples. VM carried out sea surface temperature measurements of SO202-18-3/6.
771 GM designed the study. All authors participated in the discussion of results and
772 conclusions and contributed to the final version of the paper.

773 **Competing interests**

774 The authors declare that they have no conflict of interest.

775 **Acknowledgments**

776 We thank the masters and crews of R/V Sonne for their professional support during
777 cruises SO202 (INOPEX) and SO178 (KOMEX). Hartmut Kuehn is acknowledged
778 for providing total organic carbon and dry bulk density data of site SO202-18-3/6.
779 Mengli Cao thanks the China Scholarship Council (CSC) and POLMAR- Helmholtz
780 Graduate School for Polar and Marine Research for additional support. We are also
781 grateful to the laboratory and computer staff at Alfred Wegener Institute. The
782 biomarker data generated in this study are accessible at the database Pangaea:
783 <https://doi.org/10.1594/PANGAEA.948376>.

References

784 Amon, R. M. W., Rinehart, A. J., Duan, S., Louchouart, P., Prokushkin, A., Guggenberger, G.,
785 Bauch, D., Stedmon, C., Raymond, P.A., Holmes, R. M., McClelland, J. W., Peterson, B. J.,

786 Walker, S. A., and Zhulidov, A. V.: Dissolved organic matter sources in large Arctic rivers,
787 *Geochim. Cosmochim. Ac.*, 94, 217–237, <http://dx.doi.org/10.1016/j.gca.2012.07.015>, 2012.

788 An, Z., Porter, S. C., Kutzbach, J. E., Wu, X., Wang, S., Liu, X., Li, X., and Zhou, W.:
789 Asynchronous Holocene optimum of the east Asian monsoon, *Quaternary Sci. Rev.*, 19, 743–
790 762, [https://doi.org/10.1016/S0277-3791\(99\)00031-1](https://doi.org/10.1016/S0277-3791(99)00031-1), 2000.

791 Anderson, P. M., Edwards, M. E., and Brubaker, L. B.: Results and paleoclimate implications of
792 35 years of paleoecological research in Alaska, in: *The Quaternary Period in the United*
793 *States*, edited by: Gillespie, A. R., Porter, S. C., and Atwater, B. F., Elsevier, Amsterdam,
794 427–440, [https://doi.org/10.1016/S1571-0866\(03\)01019-4](https://doi.org/10.1016/S1571-0866(03)01019-4), 2003.

795 Ballantyne, A. P., Axford, Y., Miller, G. H., Otto-Bliesner, B. L., Rosenbloom, N., and White, J. W.
796 C.: The amplification of Arctic terrestrial surface temperatures by reduced sea-ice extent
797 during the Pliocene, *Palaeogeogr. Palaeocl.*, 386, 59–67,
798 <http://dx.doi.org/10.1016/j.palaeo.2013.05.002>, 2013.

799 Bazarova, V. B., Klimin, M. A., Mokhova, L. M., and Orlova, L. A.: New pollen records of Late
800 Pleistocene and Holocene changes of environment and climate in the Lower Amur River
801 basin, NE Eurasia, *Quatern. Int.*, 179, 9–19, <https://doi.org/10.1016/j.quaint.2007.08.015>,
802 2008.

803 Belt, S. T., Massé, G., Rowland, S. J., Poulin, M., Michel, C., and LeBlanc, B.: A novel chemical
804 fossil of palaeo sea ice: IP₂₅, *Org. Geochem.*, 38, 16–27,
805 <https://doi.org/10.1016/j.orggeochem.2006.09.013>, 2007.

806 Bigelow, N. H.: Pollen Records, Late Pleistocene | Northern North America, in: *Encyclopedia of*
807 *Quaternary Science (second Edition)*, edited by: Elias, S. A., Mock, C. J., Elsevier, 39–51,
808 <https://doi.org/10.1016/B978-0-444-53643-3.00187-4>, 2013.

809 Binney, H. A., Willis, K. J., Edwards, M. E., Bhagwat, S. A., Anderson, P. M., Andreev, A. A.,
810 Blaauw, M., Damblon, F., Haesaerts, P., Kienast, F., Kremenetski, K. V., Krivonogov, S. K.,
811 Lozhkin, A. V., Macdonald, G. M., Novenko, E. Y., Oksanen, P., Sapelko, T. V., Väiliranta, M.,
812 and Vazhenina, L.: The distribution of late-Quaternary woody taxa in northern Eurasia:
813 evidence from a new macrofossil database, *Quaternary Sci. Rev.*, 28, 2445–2464,
814 <https://doi.org/10.1016/j.quascirev.2009.04.016>, 2009.

815 Brown, J., Ferrians, O., Heginbottom, J. A., and Melnikov, E.: Circum-Arctic Map of Permafrost
816 and Ground-Ice Conditions, version 2, Boulder, Colorado USA, NSIDC: National Snow and
817 Ice Data Center [data set], <https://doi.org/10.7265/skbg-kf16>, 2002.

818 Bröder, L., Tesi, T., Andersson, A., Semiletov, I., and Gustafsson, Ö.: Bounding cross-shelf
819 transport time and degradation in Siberian-Arctic land-ocean carbon transfer, *Nat. Commun.*,
820 9, 806, <https://doi.org/10.1038/s41467-018-03192-1>, 2018.

821 Caissie, B. E., Brigham-Grette, J., Lawrence, K. T., Herbert, T. D., and Cook, M. S.: Last Glacial
822 Maximum to Holocene sea surface conditions at Umnak Plateau, Bering Sea, as inferred
823 from diatom, alkenone, and stable isotope records, *Paleoceanography*, 25, PA1206,
824 <https://doi.org/10.1029/2008PA001671>, 2010.

825 Clark, P. U., Shakun, J. D., Baker, P. A., Bartlein, P. J., Brewer, S., Brook, E., Carlson, A. E.,
826 Cheng, H., Kaufman, D. S., Liu, Z., Marchitto, T. M., Mix, A. C., Morrill, C., Otto-Bliesner,
827 B. L., Pahnke, K., Russell, J. M., Whitlock, C., Adkins, J. F., Blois, J. L., Clark, J., Colman, S.
828 M., Curry, W. B., Flower, B. P., He, F., Johnson, T. C., Lynch-Stieglitz, J., Markgraf, V.,
829 McManus, J., Mitrovica, J. X., Moreno, P. I., and Williams, J. W.: Global climate evolution
830 during the last deglaciation, *P. Natl. Acad. Sci. USA*, 109, E1134–E1142,
831 <https://doi.org/10.1073/pnas.1116619109>, 2012.

832 Couture, N. J., Irragang, A., Pollard, W., Lantuit, H., and Fritzs, M.: Coastal erosion of permafrost
833 soils along the Yukon Coastal Plain and fluxes of organic carbon to the Canadian Beaufort
834 Sea, *J. Geophys. Res.-Biogeol.*, 123, 406–422, <https://doi.org/10.1002/2017JG004166>, 2018.

835 Dullo, W. C., Biebow, N., and Georgeleit, K.: SO178-KOMEX Cruise Report: Mass Exchange
836 Processes and Balances in the Okhotsk Sea, GEOMAR Report, Germany, 110 pp., 2004.

837 Dyke, A. S.: An outline of North American deglaciation with emphasis on central and northern
838 Canada, in: *Developments in Quaternary Sciences*, edited by: Ehlers, J., Gibbard, P. L.,
839 Elsevier, volume 2, part B, 373–424, [https://doi.org/10.1016/S1571-0866\(04\)80209-4](https://doi.org/10.1016/S1571-0866(04)80209-4), 2004.

840 Eglinton, G. and Hamilton, R. J.: Leaf epicuticular waxes: The waxy outer surfaces of most plants
841 display a wide diversity of fine structure and chemical constituents, *Science*, 156, 1322–1335,
842 <https://doi.org/10.1126/science.156.3780.1322>, 1967.

843 Ertel, J. R. and Hedges, J. I.: Sources of sedimentary humic substances: vascular plant debris,
844 *Geochim. Cosmochim. Acta*, 49, 2097–2107, [https://doi.org/10.1016/0016-7037\(85\)90067-5](https://doi.org/10.1016/0016-7037(85)90067-5),
845 1985.

846 Feng, X., Vonk, J. E., van Dongend, B. E., Gustafssone, Ö., Semiletov, I. P., Dudarev, O. V., Wang,
847 Z., Montlucon, D. B., Wacker, L., and Eglinton, T. I.: Differential mobilization of terrestrial
848 carbon pools in Eurasian Arctic river basins, *P. Natl. Acad. Sci. USA*, 110, 14168–14173,
849 <https://doi.org/10.1073/pnas.1307031110>, 2013.

850 Feng, X., Gustafssone, Ö., Holmes, R.M., Vonk, J. E., van Dongend, B. E., Semiletov, I. P.,
851 Dudarev, O. V., Yunker, M. B., Macdonald, R. W., Montlucon, D. B., and Eglinton, T. I.:
852 Multi-molecular tracers of terrestrial carbon transfer across the pan-Arctic: comparison of
853 hydrolyzable components with plant wax lipids and lignin phenols, *Biogeosciences*, 12,
854 4841–4860, <https://doi.org/10.5194/bg-12-4841-2015>, 2015.

855 Ficken, K. J., Li, B., Swain, D. L., and Eglinton, G.: An *n*-alkane proxy for the sedimentary input
856 of submerged/floating freshwater aquatic macrophytes, *Org. Geochem.*, 31, 745–749.
857 [https://doi.org/10.1016/S0146-6380\(00\)00081-4](https://doi.org/10.1016/S0146-6380(00)00081-4), 2000.

858 Friedlingstein, P. et al.: Global carbon budget 2020, Supplemental data of Global Carbon Budget
859 2020 (Version 1.0) [Data set], 12, 3269–3340, <https://doi.org/10.5194/essd-12-3269-2020>,
860 2020.

861 Fritz, M., Herzschuh, U., Wetterich, S., Lantuit, H., De Pascale, G. P., Pollard, W. H., and
862 Schirmer, L.: Late glacial and Holocene sedimentation, vegetation, and climate history
863 from easternmost Beringia (northern Yukon Territory, Canada), *Quaternary Res.*, 78, 549–
864 560, <http://dx.doi.org/10.1016/j.yqres.2012.07.007>, 2012.

865 Gersonde, R.: The expedition of the research vessel "Sonne" to the subpolar North Pacific and the
866 Bering Sea in 2009 (SO202-INOPEX), *Berichte zur Polar- und Meeresforschung/ Reports on
867 polar and marine research*, Bremerhaven, Alfred Wegener Institute for Polar and Marine
868 Research, 643, 323 pp, 2012.

869 Goñi, M. A., Nelson, B., Blanchette, R. A., and Hedges, J. I.: Fungal degradation of wood lignins:
870 geochemical perspectives from CuO-derived phenolic dimers and monomers, *Geochim.
871 Cosmochim. Ac.*, 57, 3985–4002, [https://doi.org/10.1016/0016-7037\(93\)90348-Z](https://doi.org/10.1016/0016-7037(93)90348-Z), 1993.

872 Goñi, M. A. and Montgomery, S.: Alkaline CuO Oxidation with a Microwave Digestion System:
873 Lignin Analyses of Geochemical Samples, *Anal. Chem.*, 72, 3116–3121,
874 <https://doi.org/10.1021/ac991316w>, 2000a.

875 Goñi, M. A., Yunker, M. B., Macdonald, R. W., Eglinton, T. I.: Distribution and sources of organic
876 biomarkers in arctic sediments from the Mackenzie River and Beaufort Shelf, *Mar. Chem.*,
877 71, 23–51, [https://doi.org/10.1016/S0304-4203\(00\)00037-2](https://doi.org/10.1016/S0304-4203(00)00037-2), 2000b.

878 Hedges, J. I. and Mann, D. C.: The characterization of plant tissues by their lignin oxidation
879 products, *Geochim. Cosmochim. Acta*, 43, 1803–1807, [https://doi.org/10.1016/0016-7037\(79\)90028-0](https://doi.org/10.1016/0016-7037(79)90028-0), 1979.

881 Hedges, J. I., Blanchette, R. A., Weliky, K., and Devol, A. H.: Effects of fungal degradation on the
882 CuO oxidation products of lignin: A controlled laboratory study, *Geochim. Cosmochim. Ac.*,
883 52, 2717–2726, [https://doi.org/10.1016/0016-7037\(88\)90040-3](https://doi.org/10.1016/0016-7037(88)90040-3), 1988.

884 Holmes, R. M., McClelland, J. W., Peterson, B. J., Tank, S. E., Bulygina, E., Eglinton, T. I.,
885 Gordeev, V. V., Gurtovaya, T. Y., Raymond, P. A., Repeta, D. J., Staples, R., Striegl, R. G.,
886 Zhulidov, A. V., and Zimov, S. A.: Seasonal and Annual Fluxes of Nutrients and Organic
887 Matter from Large Rivers to the Arctic Ocean and Surrounding Seas, *Estuar. Coasts*, 35, 369–
888 382, <https://doi.org/10.1007/s12237-011-9386-6>, 2012.

889 Hopmans, E. C., Weijers, J. W., Schefuß, E., Herfort, L., Sinninghe Damsté, J. S.y, and Schouten,
890 S.: A novel proxy for terrestrial organic matter in sediments based on branched and
891 isoprenoid tetraether lipids, *Earth Planet. Sci. Lett.*, 224, 107–116,
892 <https://doi.org/10.1016/j.epsl.2004.05.012>, 2004.

893 Hu, F. S., Hedges, J. I., Gordon, E. S., and Brubaker, L. B.: Lignin biomarkers and pollen in
894 postglacial sediments of an Alaskan lake, *Geochim. Cosmochim. Ac.*, 63, 1421–1430,
895 [https://doi.org/10.1016/S0016-7037\(99\)00100-3](https://doi.org/10.1016/S0016-7037(99)00100-3), 1999.

896 Hugelius, G., Strauss, J., Zubrzycki, S., Harden, J. W., Schuur, E. A. G., Ping, C.-L., Schirmermeister,
897 L., Grosse, G., Michaelson, G. J., Koven, C. D., O'Donnell, J. A., Elberling, B., Mishra, U.,
898 Camill, P., Yu, Z., Palmtag, J., and Kuhry, P.: Estimated stocks of circumpolar permafrost
899 carbon with quantified uncertainty ranges and identified data gaps, *Biogeosciences*, 11,
900 6573–6593, <https://doi.org/10.5194/bg-11-6573-2014>, 2014.

901 Igarashi, Y. and Zharov, A. E.: Climate and vegetation change during the late Pleistocene and early
902 Holocene in Sakhalin and Hokkaido, northeast Asia, *Quaternary Int.*, 237, 24–31,
903 <https://doi.org/10.1016/j.quaint.2011.01.005>, 2011.

904 Irrgang, A. M., Bendixen, M., Farquharson, L. M., Baranskaya, A. V., Erikson, L. H., Gibbs, A. E.,
905 Ogorodov, S. A., Overduin, P. P., Lantuit, H., Grigoriev, M. N., Jones, B. M.: Drivers,
906 dynamics and impacts of changing Arctic coasts, *Nat. Rev. Earth Environ.*, 3, 39–54,
907 <https://doi.org/10.1038/s43017-021-00232-1>, 2022.

908 Jakobsson, M., Pearce, C., Cronin, T. M., Backman, J., Anderson, L. G., Barrientos, N., Björk, G.,
909 Coxall, H., de Boer, A., Mayer, L. A., Mörth, C.-M., Nilsson, J., Rattray, J. E., Stranne, C.,
910 Semiletov, I., and O'Regan, M.: Post-glacial flooding of the Bering land bridge dated to 11
911 cal ka BP based on new geophysical and sediment records, *Clim. Past*, 13, 991–1005,
912 <https://doi.org/10.5194/cp-13-991-2017>, 2017.

913 Jones, M. C., Berkelhammer, M., Keller, K. J., Yoshimura, K., and Wooller, M. J.: High sensitivity
914 of Bering Sea winter sea ice to winter insolation and carbon dioxide over the last 5500 years,
915 *Science Advances*, 6, eaaz9588, 2020.

916 Kaufman, D. S., Axford, Y. L., Henderson, A. C. G., McKay, N. P., Oswald, W. W., Saenger, C.,
917 Anderson, R. S., Bailey, H. L., Clegg, B., Gajewski, K., Hu, F. S., Jones, M. C., Massa, C.,
918 Routson, C. C., Werner, A., Wooller, M. J., and Yu, Z.: Holocene climate changes in eastern
919 Beringia (NW North America)-A systematic review of multi-proxy evidence, *Quaternary Sci.*
920 *Rev.*, 312–339, <https://doi.org/10.1016/j.quascirev.2015.10.021>, 2015.

921 Kennedy, K. E., Froese, D. G., Zazula, G. D., Lauriol, B.: Last glacial maximum age for the
922 northwest Laurentide maximum from the eagle river spillway and delta complex, northern
923 Yukon, *Quat. Sci. Rev.* 29, 1288–300, <https://doi.org/10.1016/j.quascirev.2010.02.015>, 2010.

924 Keskitalo, K., Tesi, T., Bröder, L., Andersson, A., Pearce, C., Sköld, M., Semiletov, I. P., Dudarev,
925 O. V., and Gustafsson, Ö.: Sources and characteristics of terrestrial carbon in Holocene-scale
926 sediments of the East Siberian Sea, *Clim. Past*, 13, 1213–1226, <https://doi.org/10.5194/cp-13-1213-2017>, 2017.

928 Kim, J.-H., Schouten, S., Hopmans, E. C., Donner, B., and Sinninghe Damsté, J. S.: Global
929 sediment core-top calibration of the TEX₈₆ paleothermometer in the ocean, *Geochim.*
930 *Cosmochim. Acta*, 72, 1154–1173, <https://doi.org/10.1016/j.gca.2007.12.010>, 2008.

931 Kim, J.-H., van der Meer, J., Schouten, S., Helmke, P., Willmott, V., Sangiorgi, F., Koç, N.,
932 Hopmans, E. C., and Sinninghe Damsté, J. S.: New indices and calibrations derived from the
933 distribution of crenarchaeal isoprenoid tetraether lipids: Implications for past sea surface
934 temperature reconstructions, *Geochim. Cosmochim. Ac.*, 74, 4639–4654,
935 <https://doi.org/10.1016/j.gca.2010.05.027>, 2010.

936 Kuehn, H., Lembke-Jene, L., Gersonde, R., Esper, O., Lamy, F., Arz, H., Kuhn, G., and
937 Tiedemann, R.: Laminated sediments in the Bering Sea reveal atmospheric teleconnections to
938 Greenland climate on millennial to decadal timescales during the last deglaciation, *Clim. Past*,
939 10, 2215–2236, <https://doi.org/10.5194/cp-10-2215-2014>, 2014.

940 Lambeck, K., Rouby, H., Purcell, A., Sun, Y., and Sambridge, M.: Sea level and global ice
941 volumes from the Last Glacial Maximum to the Holocene, *P. Natl. Acad. Sci. USA*, 11,
942 15296–15303, <https://doi.org/10.1073/pnas.1411762111>, 2014.

943 Lantuit, H., Overduin, P.P., Couture, N., Wetterich, S., Aré, F., Atkinson, D., Brown, J.,
944 Cherkashov, G., Drozdov, D., Forbes, D.L., Graves-Gaylord, A., Grigoriev, M., Hubberten,
945 H.-W., Jordan, J., Jorgenson, T., Ødegård, R. S., Ogorodov, S., Pollard, W. H., Rachold, V.,
946 Sedenko, S., Solomon, S., Steenhuisen, F., Streletskaia, I., and Vasilev, A.: The Arctic
947 Coastal Dynamics Database: A New Classification Scheme and Statistics on Arctic
948 Permafrost Coastlines, *Estuar. Coasts*, 35, 383–400, <https://doi.org/10.1007/s12237-010-9362-6>, 2012.

950 Lattaud, J., Lo, L., Zeeden, C., Liu, Y.-J., Song, S.-R., van der Meer, M. T. J., Damsté, J. S. S., and
951 Schouten, S.: A multiproxy study of past environmental changes in the Sea of Okhotsk during

952 the last 1.5 Ma, *Org. Geochem.*, 132, 50–61,
953 <https://doi.org/10.1016/j.orggeochem.2019.04.003>, 2019.

954 Lawrence, D. M., Slater, A. G., Tomas, R. A., Holland, M. M., and Deser, C.: Accelerated Arctic
955 land warming and permafrost degradation during rapid sea ice loss, *Geophys. Res. Lett.*, 35,
956 L11506, <https://doi.org/10.1029/2008GL033985>, 2008.

957 Lembke-Jene, L., Tiedemann, R., Nürnberg, D., Kokfelt, U., Kozdon, R., Max, L., Röhl, U., and
958 Gorbarenko, S. A.: Deglacial variability in Okhotsk Sea Intermediate Water ventilation and
959 biogeochemistry: Implications for North Pacific nutrient supply and productivity, *Quat. Sci.
960 Rev.*, 160, 116–137, <https://doi.org/10.1016/j.quascirev.2017.01.016>, 2017.

961 Liu, J., Curry, J. A., Wang, H., Song, M., and Horton, R. M.: Impact of declining Arctic sea ice on
962 winter snowfall, *Proc. Natl Acad. Sci. USA*, 109, 4074–4079,
963 <https://doi.org/10.1073/pnas.111491010>, 2012.

964 Lo, L., Belt, S. T., Lattaud, J., Friedrich, T., Zeeden, C., Schouten, S., Smik, L., Timmermann, A.,
965 Cabedo-Sanz, P., Huang, J.-J., Zhou, L., Ou, T.-H., Chang, Y.-P., Wang, L.-C., Chou, Y.-M.,
966 Shen, C.-C., Chen, M.-T., Wei, K.-Y., Song, S.-R., Fang, T.-H., Gorbarenko, S. A., Wang, W.-
967 L., Lee, T.-Q., Elderfield, H., and Hodell, D. A.: Precession and atmospheric CO₂ modulated
968 variability of sea ice in the central Okhotsk Sea since 130,000 years ago, *Earth Planet. Sc.
969 Lett.*, 488, 36–45, <https://doi.org/10.1016/j.epsl.2018.02.005>, 2018.

970 Lobbes, J., Fitznar, H. P., and Kattner, G.: Biogeochemical characteristics of dissolved and
971 particulate organic matter in Russian rivers entering the Arctic Ocean, *Geochim. Cosmochim.
972 Ac.*, 64, 2973 – 2983, [https://doi.org/10.1016/S0016-7037\(00\)00409-9](https://doi.org/10.1016/S0016-7037(00)00409-9), 2000.

973 Manley, W. F.: Postglacial flflooding of the bering land bridge: a geospatial animation: INSTAAR,
974 University of Colorado, v1, http://instaar.colorado.edu/QGISL/bering_land_bridge, 2002.

975 Martens, J., Wild, B., Pearce, C., Tesi, T., Andersson, A., Bröder, L., O’Regan, M., Jacobsson, M.,
976 Sköld, M., Gemery, L., Cronin, T. M., Semiletov, I., Dudarev, O. V., and Gustafsson, Ö.:
977 Remobilization of old permafrost carbon to Chukchi Sea sediments during the end of the last
978 deglaciation, *Global Biogeochem. Cy.*, 33, 2–14, <https://doi.org/10.1029/2018GB005969>,
979 2019.

980 Martens, J., Wild, B., Muschitiello, F., O’Regan, M., Jacobsson, M., Semiletov, I., Dudarev, O. V.,
981 and Gustafsson, Ö.: Remobilization of dormant carbon from Siberian-Arctic permafrost
982 during three past warming events, *Science Advances*, 6, eabb6546, 2020.

983 Max, L., Riethdorf, J.-R., Tiedemann, R., Smirnova, M., Lembke-Jene, L., Fahl, K., Nürnberg, D.,
984 Matul, A., and Mollenhauer, G.: Sea surface temperature variability and sea-ice extent in the
985 subarctic northwest Pacific during the past 15,000 years, *Paleoceanography*, 27, PA3213,
986 <https://doi.org/10.1029/2012PA002292>, 2012.

987 Max, L., Lembke-Jene, L., Riethdorf, J.-R., Tiedemann, R., Nürnberg, D., and Mackensen, A.:
988 Pulses of enhanced North Pacific Intermediate Water ventilation from the Okhotsk Sea and
989 Bering Sea during the last deglaciation, *Clim. Past*, 10, 591–605, [https://doi.org/10.5194/cp-
990 10-591-2014](https://doi.org/10.5194/cp-10-591-2014), 2014.

991 Méheust, M., Stein, R., Fahl, K., Max, L., and Riethdorf, J. R.: High-resolution IP₂₅-based
992 reconstruction of sea-ice variability in the western North Pacific and Bering Sea during the
993 past 18,000 years, *Geo-Mar. Lett.*, 36, 101–111, <https://doi.org/10.1007/s00367-015-0432-4>,
994 2016.

995 Méheust, M., Stein, R., Fahl, K., and Gersonde, R.: Sea-ice variability in the subarctic North
996 Pacific and adjacent Bering Sea during the past 25 ka: new insights from IP₂₅ and U^k₃₇ proxy
997 records, *Arktos*, 4, 1–19, <https://doi.org/10.1007/s41063-018-0043-1>, 2018.

998 Menard, E., Allard, M., and Michaud, Y.: Monitoring of ground surface temperatures in various
999 biophysical micro-environments near Umiujaq, eastern Hudson Bay, Canada, in *Proceedings
1000 of the 7th International Conference on Permafrost*, June 23–27, Yellowknife, Canada,
1001 Nordicana, vol. 57, edited by Lewkowicz, A. G. and Allard, M., pp. 723–729, Univ. Laval,
1002 Quebec, Que., Canada, 1998.

1003 Meyer, V. D., Max, L., Hefter, J., Tiedemann, R., and Mollenhauer, G.: Glacial-to-Holocene
1004 evolution of sea surface temperature and surface circulation in the subarctic northwest
1005 Pacific and the Western Bering Sea, *Paleoceanography*, 31, 916–927,
1006 <https://doi.org/10.1002/2015PA002877>, 2016.

1007 Meyer, V. D., Hefter, J., Lohmann, G., Max, L., Tiedemann, R., and Mollenhauer, G.: Summer
1008 temperature evolution on the Kamchatka Peninsula, Russian Far East, during the past 20 000
1009 years, *Clim. Past*, 13, 359–377, <https://doi.org/10.5194/cp-13-359-2017>, 2017.

1010 Meyer, V. D., Hefter, J., Köhler, P., Tiedemann, R., Gersonde, R., Wacker, L., and Mollenhauer,
1011 G.: Permafrost-carbon mobilization in Beringia caused by deglacial meltwater runoff, sea-
1012 level rise and warming, *Environ. Res. Lett.*, 14, 085003, <https://doi.org/10.1088/1748-9326/ab2653>, 2019.

1014 Morley, J. J., Heusser, L. E., and Shackleton, N. J.: Late Pleistocene/Holocene radiolarian and
1015 pollen records from sediments in the Sea of Okhotsk, *Paleoceanography*, 6, 121–131,
1016 <https://doi.org/10.1029/90PA02031>, 1991.

1017 Nakatsuka, T., Toda, M., Kawamura, K., and Wakatsuchi, M.: Dissolved and particulate organic
1018 carbon in the Sea of Okhotsk: Transport from continental shelf to ocean interior, *J. Geophys.*
1019 *Res.*, 109, C09S14, <https://doi.org/10.1029/2003JC001909>, 2004.

1020 Otto, A. and Simpson, M. J.: Degradation and preservation of vascular plant-derived biomarkers in
1021 grassland and forest soils from Western Canada, *Biogeosciences*, 74, 377–409,
1022 <https://doi.org/10.1007/s10533-004-5834-8>, 2005.

1023 Otto, A., and Simpson, M. J.: Evaluation of CuO oxidation parameters for determining the source
1024 and stage of lignin degradation in soil, *Biogeochemistry*, 80, 121–142,
1025 <https://doi.org/10.1007/s10533-006-9014-x>, 2006.

1026 Park, H., Walsh, J. E., Kim, Y., Nakai, T., and Ohata, T.: The role of declining Arctic sea ice in
1027 recent decreasing terrestrial Arctic snow depths, *Polar Sci.*, 7, 174–187,
1028 <https://doi.org/10.1016/j.polar.2012.10.002>, 2013.

1029 Praetorius, S. K., Mix, A. C., Walczak, M. H., Wohowe, M. D., Addison, J. A., and Prahl, F. G.:
1030 North Pacific deglacial hypoxic events linked to abrupt ocean warming, *Nature*, 527, 362–
1031 366, <https://doi.org/10.1038/nature15753>, 2015.

1032 Rasmussen, S. O., Seierstad, I. K., Andersen, K. K., Bigler, M., Dahl-Jensen, D., and Johnsen, S.
1033 J.: Synchronization of the NGRIP, GRIP, and GISP2 ice cores across MIS 2 and
1034 palaeoclimatic implications, *Quaternary Sci. Rev.*, 27, 18–28,
1035 <https://doi.org/10.1016/j.quascirev.2007.01.016>, 2008.

1036 Riethdorf, J.-R., Max, L., Nürnberg, D., Lembke-Jene, L., and Tiedemann, R.: Deglacial history of
1037 (sub) sea surface temperatures and salinity in the subarctic NW Pacific: implications for
1038 upper-ocean stratification, *Paleoceanography* 28, 91e104, <https://doi.org/10.1002/palo.20014>,
1039 2013.

1040 Schirrneister, L., Froese, D., Tumskey, V., Grosse, G., and Wetterich, S.: Yedoma: Late
1041 Pleistocene ice-rich syngenetic permafrost of Beringia, in: *Encyclopedia of Quaternary*
1042 *Science* (second edition), edited by: Elias, S. A. and Mock, C. J., Elsevier, Amsterdam, 542–
1043 552, <https://doi.org/10.1016/B978-0-444-53643-3.00106-0>, 2013.

1044 Schouten, S., Hopmans, E. C., Schefuß, E., and Sinninghe Damsté, J. S.: Distributional variations
1045 in marine crenarchaeotal membrane lipids: A new tool for reconstructing ancient sea water
1046 temperatures?, *Earth Planet. Sci. Lett.*, 204, 265–274, [https://doi.org/10.1016/S0012-821X\(02\)00979-2](https://doi.org/10.1016/S0012-821X(02)00979-2), 2002.

1048 Schuur, E. A. G., McGuire, A. D., Schädel, C., Grosse, G., Harden, J. W., Hayes, D. J., Hugelius,
1049 G., Koven, C. D., Kuhry, P., Lawrence, D. M., Natali, S. M., Olefeld, D., Romanovsky, V. E.,
1050 Schaefer, K., Turetsky, M. R., Treat, C. C., and Vonk, J. E.: Climate change and the
1051 permafrost carbon feedback, *Nature*, 520, 171–179, <https://doi.org/10.1038/nature14338>,
1052 2015.

1053 Schweger, C., Froese, D., White, J. M., and Westgate, J. A.: Pre-glacial and interglacial pollen
1054 records over the last 3 Ma from northwest Canada: Why do Holocene forests differ from
1055 those of previous interglaciations?, *Quaternary Sci. Rev.*, 30, 2124–2133.
1056 <https://doi.org/10.1016/j.quascirev.2011.01.020>, 2011.

1057 Seki, O., Harada, N., Sato, M., Kawamura, K., Ijiri, A., and Nakatsuka, T.: Assessment for
1058 paleoclimatic utility of terrestrial biomarker records in the Okhotsk Sea sediments, *Deep-Sea*
1059 *Res. Pt. II*, 85–92, <https://doi.org/10.1016/j.dsr2.2011.03.008>, 2012.

1060 Seki, O., Mikami, Y., Nagao, S., Bendle, J.A., Nakatsuka, T., Kim, V. I., Shesterkin, V. P., Makinov,
1061 A. N., Fukushima, M., Mossen, H. M., and Schouten, S.: Lignin phenols and BIT index
1062 distribution in the Amur River and the Sea of Okhotsk: Implications for the source and

1063 transport of particulate terrestrial OC to the Ocean, *Prog. Oceanogr.*, 126, 146-154,
1064 <http://dx.doi.org/10.1016/j.pocean.2014.05.003>, 2014a.

1065 Seki, O, Bendle, J.A., Harada, N., Kobayashi, M., Sawada, K., Moossen, H., Inglis, G.N., Nagao,
1066 S., Sakamoto, T.: Assessment and calibration of TEX₈₆ paleothermometry in the Sea of
1067 Okhotsk and sub-polar North Pacific region: Implications for paleoceanography, *Prog.*
1068 *Oceanogr.*, 126, 254-266, <http://dx.doi.org/10.1016/j.pocean.2014.04.013>, 2014b.

1069 Smith, C. A. S., Burn, C. R., Tarnocai, C., and Sproule, B.: Air and soil temperature relations
1070 along an ecological transect through the permafrost zones of northwestern Canada, in:
1071 *Proceedings of the 7th International Conference on Permafrost*, Yellowknife, Canada,
1072 Nordicana, June 23–27, vol. 57, pp. 1009–1015, edited by Lewkowicz, A. G., and Allard, M.,
1073 Univ. Laval, Quebec, Que., Canada, 1998.

1074 Strauss, J., Schirrmeister, L., Grosse, G., Wetterich, S., Ulrich, M., Herzschuh, U., and Hubberten,
1075 H. W.: The deep permafrost carbon pool of the Yedoma region in Siberia and Alaska,
1076 *Geophys. Res. Lett.*, 40, 6165–6170, <http://dx.doi.org/10.1002/2013GL058088>, 2013.

1077 Sun, S., Schefuß, E., Mulitza, S., Chiessi, C. M., Sawakuchi, A. O., Zabel, M., Baker, P. A., Hefter,
1078 J., and Mollenhauer, G.: Origin and processing of terrestrial organic carbon in the Amazon
1079 system: lignin phenols in river, shelf, and fan sediments, *Biogeosciences*, 14, 2495–2512.
1080 <https://doi.org/10.5194/bg-14-2495-2017>, 2017.

1081 Tarasov, P. E., Bezrukova, E. V., and Krivonogov, S. K.: Late Glacial and Holocene changes in
1082 vegetation cover and climate in southern Siberia derived from a 15 kyr long pollen record
1083 from Lake Kotokel, *Clim. Past*, 5, 285–295, <https://doi.org/10.5194/cp-5-285-2009>, 2009.

1084 Tesi, T., Semiletov, I., Hugelius, G., Dudarev, O., Kuhry, P., and Gustafsson, Ö.: Composition and
1085 fate of terrigenous organic matter along the Arctic land-ocean continuum in East Siberia:
1086 Insights from biomarkers and carbon isotopes, *Geochim. Cosmochim. Ac.*, 133, 235–256,
1087 <http://dx.doi.org/10.1016/j.gca.2014.02.045>, 2014.

1088 Tesi, T., Muschitiello, F., Smittenberg, R. H., Jakobsson, M., Vonk, J. E., Hill, P., Andersson, A.,
1089 Kirchner, N., Noormets, R., Dudarev, O., Semiletov, I., and Gustafsson, Ö.: Massive
1090 remobilization of permafrost carbon during post-glacial warming, *Nature Commun.*, 7, 13653,
1091 <https://doi.org/10.1038/ncomms13653>, 2016.

1092 Vaks, A., Gutareva, O. S., Breitenbach, S. F. M., Avirmed, E., Mason, A. J., Thomas, A. L.,
1093 Osinzev, A. V., Kononov, A. M., and Henderson, G. M.: Speleothems Reveal 500,000-year
1094 history of Siberian Permafrost, *Science*, 340, 183–186, 2013.

1095 Vaks, A., Mason, A. J., Breitenbach, S. F. M., Kononov, A. M., Osinzev, A. V., Rosensaft, M.,
1096 Borshevsky, A., Gutareva, O. S., and Henderson, G. M.: Palaeoclimate evidence of
1097 vulnerable permafrost during times of low sea ice, *Nature*, 577, 221–225,
1098 <https://doi.org/10.1038/s41586-019-1880-1>, 2020.

1099 Vandenberghe, J., French, H. M., Gorbunov, A., Marchenko, S., Velichko, A. A., Jin, H., Cui, Z.,
1100 Zhang, T., and Wan, X.: The Last Permafrost Maximum (LPM) map of the Northern
1101 Hemisphere: permafrost extent and mean annual air temperatures, 25–17 ka BP, *Boreas*, 43,
1102 652–666, <https://doi.org/10.1111/bor.12070>, 2014.

1103 Viau, A. E., Gajewski, K., Sawada, M. C., and Bunbury, J.: Low- and high-frequency
1104 climatevariability in eastern Beringia during the past 25 000 years, *Can. J. Earth Sci.*, 45,
1105 1435–1453, <https://doi.org/10.1139/E08-036>, 2008.

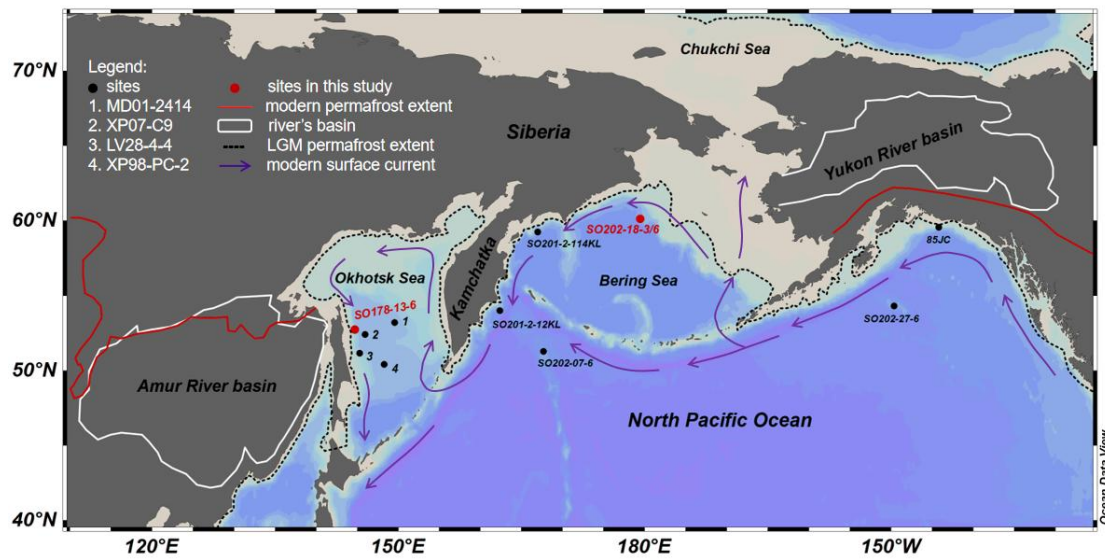
1106 Walter Anthony, K. M., Zimov, S. A., Grosse, G., Jones, M. C., Anthony, P. M., Chapin III, F. S.,
1107 Finlay, J. C., Mack, M. C., Davydov, S., Frenzel, P., and Frolking, S.: A shift of thermokarst
1108 lakes from carbon sources to sinks during the Holocene epoch, *Nature*, 511, 452–456,
1109 <https://doi.org/10.1038/nature13560>, 2014.

1110 Walter, K. M., Zimov, S. A., Chanton, J. P., Verbyla, D., and Chapin III, F. S.: Methane bubbling
1111 from Siberian thaw lakes as a positive feedback to climate warming, *Nature*, 443, 71–75,
1112 <https://doi.org/10.1038/nature05040>, 2006.

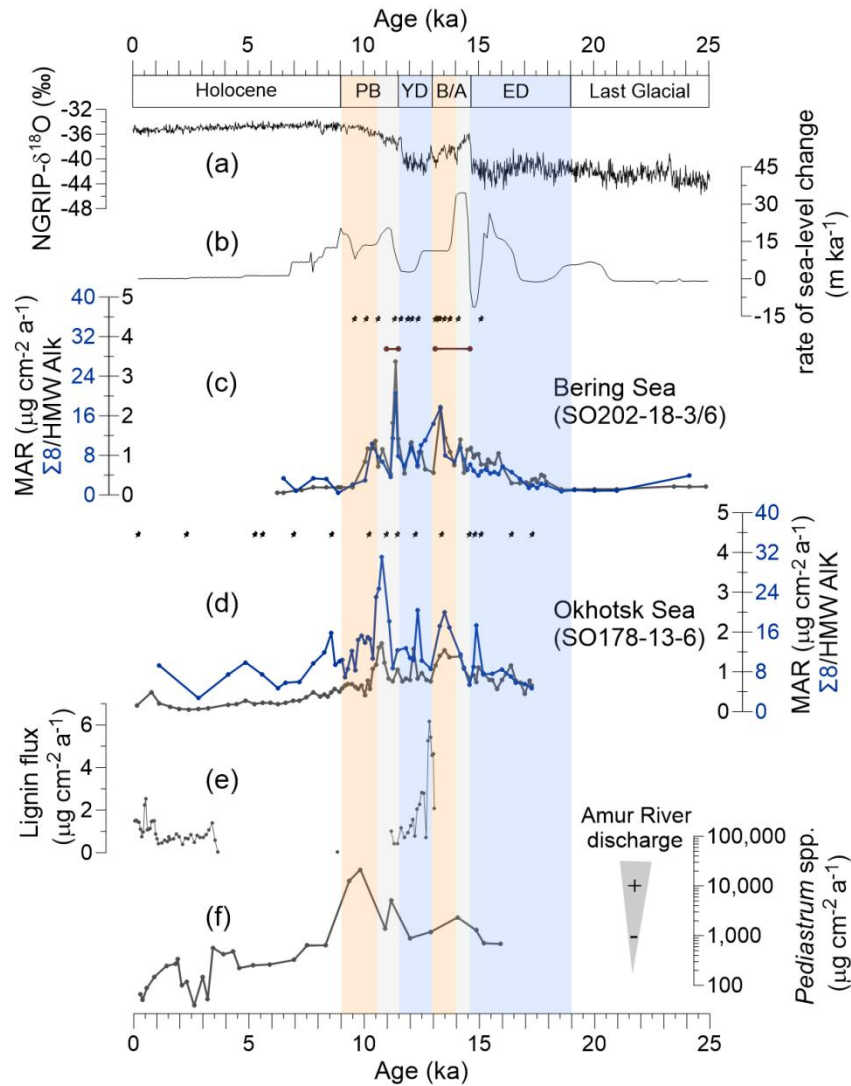
1113 Walter, K. M., Edwards, M. E., Grosse, G., Zimov, S. A., and Chapin III, F. S.: Thermokarst lakes
1114 as a source of atmospheric CH₄ during the last deglaciation, *Science*, 318, 633–636,
1115 <https://doi.org/10.1126/science.1142924>, 2007.

1116 Wang, R., Kuhn, G., Gong, X., Biskabrn, B. K., Gersonde, R., Lembke-Jene, L., Lohmann, G.,
1117 Tiedemann, R., and Diekmann, B.: Deglacial land-ocean linkages at the Alaskan continental

- 1118 margin in the Bering Sea, *Front. Earth Sci.*, 9:712415,
1119 <https://doi.org/10.3389/feart.2021.712415>, 2021.
- 1120 Weijers, J. W. H., Schouten, S., Spaargaren, O. C., and Sinninghe Damsté, J.S.: Occurrence and
1121 distribution of tetraether membrane lipids in soils: Implications for the use of the TEX₈₆
1122 proxy and the BIT index, *Org. Geochem.*, 37, 1680–1693,
1123 <https://doi.org/10.1016/j.orggeochem.2006.07.018>, 2006.
- 1124 Wild, B., Shakhova, N., Dudarev, O., Ruban, A., Kosmach, D., Tumskey, V., Tesi, T., Grimm, H.,
1125 Nybomy, I., Matsubara, F., Alexanderson, H., Jakobsson, M., Mazurov, A., Semiletov, I., and
1126 Gustafsson, Ö.: Organic matter composition and greenhouse gas production of thawing
1127 subsea permafrost in the Laptev Sea, *Nature Commun.*, 13, 5057,
1128 <https://doi.org/10.1038/s41467-022-32696-0>, 2022.
- 1129 Winterfeld, M., Goñi, M. A., Just, J., Hefter, J., and Mollenhauer, G.: Characterization of
1130 particulate organic matter in the Lena River delta and adjacent nearshore zone, NE Siberia-
1131 Part 2: Lignin-derived phenol compositions, *Biogeosciences*, 12, 2261–2283,
1132 <https://doi.org/10.5194/bg-12-2261-2015>, 2015.
- 1133 Winterfeld, M., Mollenhauer, G., Dumann, W., Köhler, P., Lembke-Jene, L., Meyer, V. D.,
1134 Hefter, J., McIntyre, C., Wacker, L., Kokfelt, U., and Tiedemann, R.: Deglacial mobilization
1135 of pre-aged terrestrial carbon from degrading permafrost, *Nature Commun.*, 9, 3666,
1136 <https://doi.org/10.1038/s41467-018-06080-w>, 2018.
- 1137 Wu, J., Mollenhauer, G., Stein, R., Köhler, P., Hefter, J., Fahl, K., Grotheer, H., Wei, B., and Nam,
1138 S.: Deglacial release of petrogenic and permafrost carbon from the Canadian Arctic
1139 impacting the carbon cycle, *Nature Commun.*, 13, 7172, [https://doi.org/10.1038/s41467-022-](https://doi.org/10.1038/s41467-022-34725-4)
1140 [34725-4](https://doi.org/10.1038/s41467-022-34725-4), 2022.
- 1141 Yu, S.-H., Zheng, Z., Kershaw, P., Skrypnikova, M., and Huang, K.-Y.: A late Holocene record of
1142 vegetation and fire from the Amur Basin, far-eastern Russia, *Quatern. Int.*, 432, 79 – 92,
1143 <https://doi.org/10.1016/j.quaint.2014.07.059>, 2017.
- 1144 Zhang, T. Influence of the seasonal snow cover on the ground thermal regime: an overview, *Rev.*
1145 *Geophys.*, 43, RG4002, <https://doi.org/10.1029/2004RG000157>, 2005.

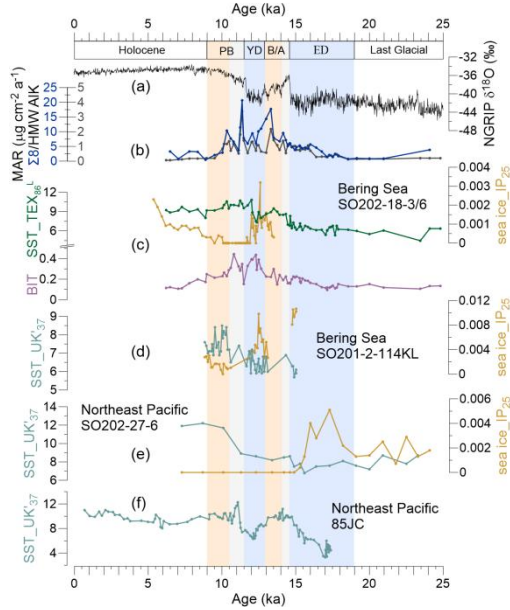


1146 **Figure 1.** Study area. Red dots indicate locations of sediment cores investigated in this study;
 1147 black dots denote cores described in previous studies. 1: site MD01-2414 (Lattaud et al., 2019;
 1148 Lo et al., 2018). 2: site XP07-C9 (Seki et al., 2012). 3: site LV28-4-4 (Winterfeld et al., 2018).
 1149 4: site XP98-PC-2 (Seki et al., 2014b).

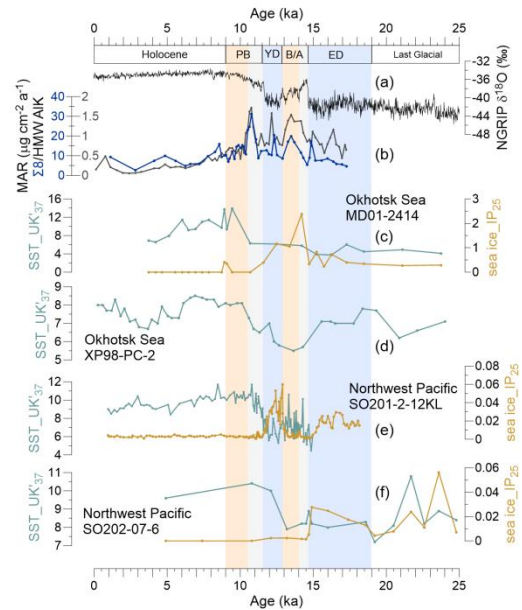


1150 **Figure 2.** Proxy records of terrestrial organic matter supply and environmental records of
 1151 deglacial changes. (a) Greenland NGRIP $\delta^{18}\text{O}$ (Rasmussen et al., 2008). (b) Global rate of
 1152 sea-level change (Lambeck et al., 2014). (c) MAR of lignin phenols (blue) and HMW Alk
 1153 (black; Meyer et al., 2019) from core SO202-18-3/6. (d) MAR of lignin phenols (blue) and
 1154 HMW Alk (black; Winterfeld et al., 2018) from core SO178-13-6. Pin marks at the top of (c)
 1155 and (d) show age control points, the accelerator mass spectrometry ^{14}C dates for SO202-18-
 1156 3/6 (Kuehn et al., 2014) and SO178-13-6 (Max et al., 2012). Brown bars in panel c indicate
 1157 laminated/layered (anoxic) core sections (Kuehn et al., 2014). (e) Lignin flux from core 4-
 1158 PC1 (Chukchi Sea, Martens et al., 2019). (f) Accumulation rate of chlorophycean freshwater
 1159 algae *Pediastrum* spp. from core LV28-4-4 (Winterfeld et al., 2018). Blue boxes represent the
 1160 cold spells the early deglaciation (ED) and Younger Dryas (YD), orange boxes are for the
 1161 warm phases Bølling-Allerød (B/A) and Pre-Boreal (PB). Gray boxes highlight the periods of
 1162 melt water pulse 1A (MWP-1A) and 1B (MWP-1B).

I. Bering Sea and Northeast Pacific



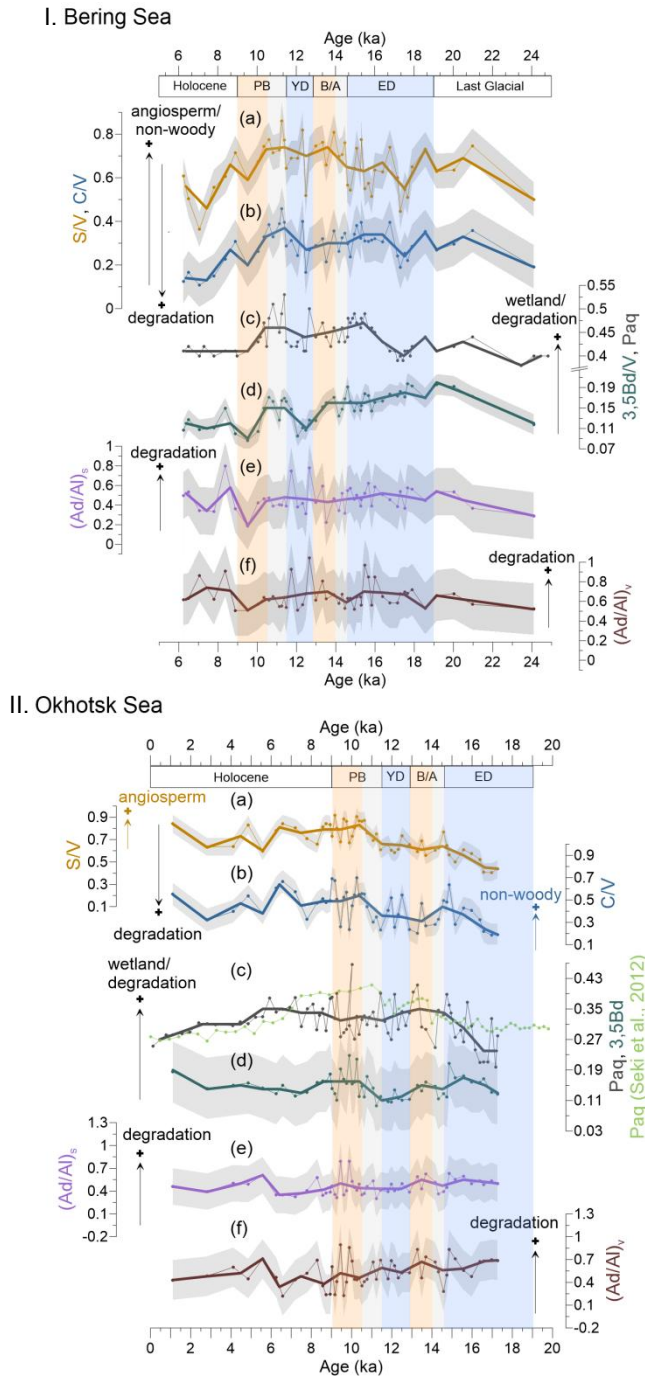
II. Okhotsk Sea and Northwest Pacific



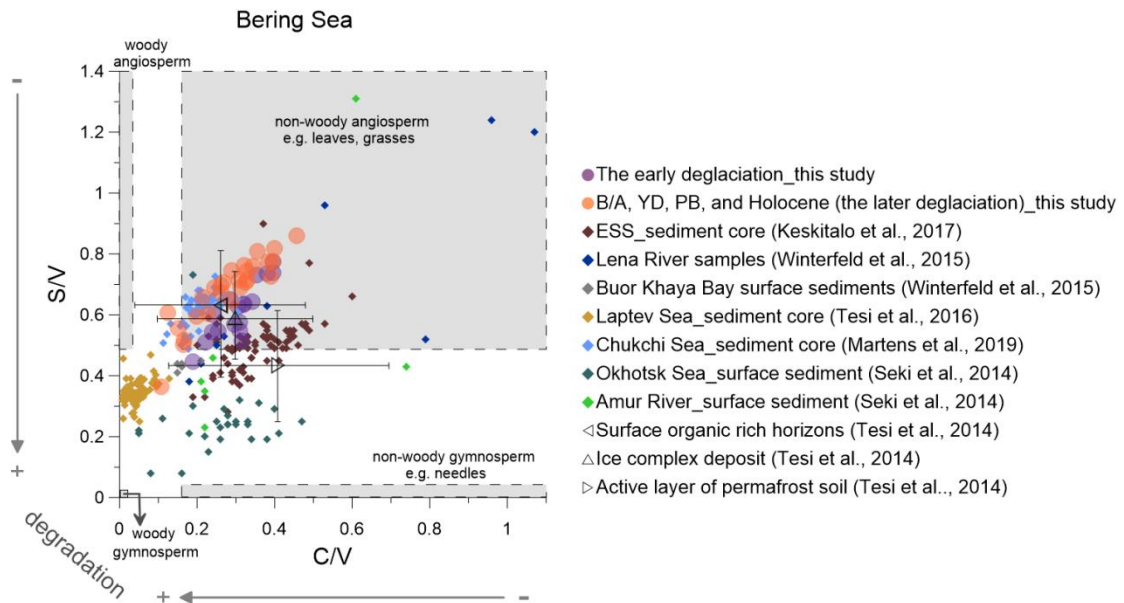
1163 **Figure 3.** Records of sea surface temperature (SST) and sea ice (IP₂₅) in the Bering Sea and
 1164 Northeast Pacific, and Okhotsk Sea and Northwest Pacific during the past 25 ka. (a) NGRIP-
 1165 $\delta^{18}\text{O}$ from Greenland (Rasmussen et al., 2008). (b) MAR of biomarkers.

1166 I: (c) The green line reflects SST (TEX₈₆^L), and the purple line shows the BIT from this study,
 1167 SO202-18-3/6. The orange line denotes the IP₂₅ obtained for this core by Méheust et al.
 1168 (2018). (d) SST and IP₂₅ for core SO202-2-114KL (Max et al., 2012; Méheust et al., 2016). (e)
 1169 SST and IP₂₅ for core SO202-27-6 in the Northeast Pacific (Méheust et al., 2018). (f) SST for
 1170 core 85JC (Praetorius et al., 2015).

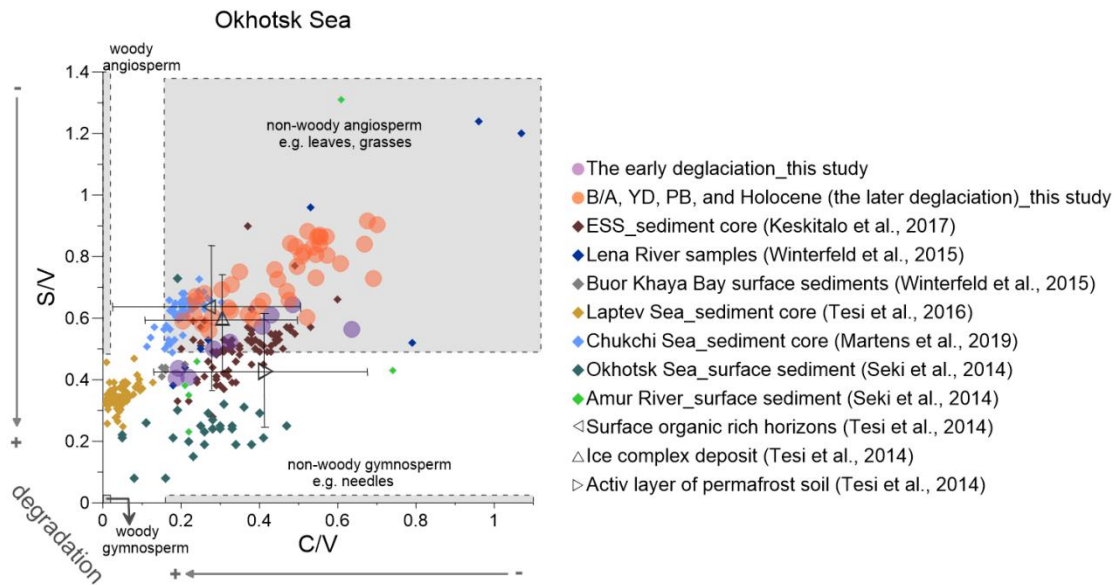
1171 II: (c) SST and IP₂₅ of the core MD01-2414 in the Okhotsk Sea (Lattaud et al., 2019; Lo et al.,
 1172 2018). (d) SST for core XP98-PC-2 (Seki et al., 2014b). (e) SST and IP₂₅ for core SO201-2-
 1173 12KL in the Northwest Pacific (Max et al., 2012; Méheust et al., 2016). (f) SST and IP₂₅ for
 1174 core SO202-07-6 (Méheust et al., 2018). The units of the SST and IP₂₅ are °C and $\mu\text{g g}^{-1}$
 1175 sediment, respectively. Blue boxes represent intervals with prevailing colder climate
 1176 conditions during the early deglaciation (ED) and Younger Dryas (YD), orange boxes are for
 1177 the warm phases Bølling-Allerød (B/A) and Preboreal (PB). Gray boxes highlight the periods
 1178 of melt water pulse 1A (MWP-1A) and 1B (MWP-1B).



1179 **Figure 4.** Records of lignin and non-lignin phenol indices compared with the Paq index in
 1180 Bering and Okhotsk Sea sediments. (a and b): S/V and C/V ratios reflect the vegetation
 1181 change and/or degree of lignin degradation in the respective river basins. (c and d): 3,5Bd/V
 1182 and Paq ratios represent the wetland extent or degree of degradation in the respective
 1183 catchments. In panel II showing records from the Okhotsk Sea, the light green line represents
 1184 the Paq of a nearby core, XP07-C9 (Seki et al., 2012). (e and f): The Ad/Al can reflect the
 1185 degradation of lignin phenols. Grey shaded areas illustrate the uncertainty of these indices.
 1186 Bold lines are the 1 ka averages of the corresponding indices. Blue boxes represent the cold
 1187 spells the early deglaciation (ED) and Younger Dryas (YD), orange boxes are for the warm
 1188 phases Bølling-Allerød (B/A) and Pre-Boreal (PB). Gray boxes highlight the periods of melt
 1189 water pulse 1A (MWP-1A) and 1B (MWP-1B).



1190 **Figure 5.** Lignin indicators of terrigenous material in the Bering sediment (solid circles)
 1191 compared with previously studied (Martens et al., 2019; Keskitalo et al., 2017; Tesi et al.,
 1192 2016; Seki et al., 2014a; Winterfeld et al., 2015). The early deglaciation is from 19 to 14.6 ka
 1193 BP and after the early deglaciation is the later deglaciation. The dark triangles represent the
 1194 ratio of S/V and C/V from surface soils, Ice Complex deposits and active layer permafrost
 1195 (Tesi et al., 2014). ESS is short for the East Siberian Shelf.



1196 **Figure 6.** Lignin indicators of terrigenous material in the Okhotsk Sea sediment (solid circles)
 1197 compared with previously studied (Martens et al., 2019; Keskitalo et al., 2017; Tesi et al.,
 1198 2016; Seki et al., 2014a; Winterfeld et al., 2015). The early deglaciation is from 19 to 14.6 ka
 1199 BP and after the early deglaciation is the later deglaciation. The dark triangles represent the
 1200 ratio of S/V and C/V from surface soils, Ice Complex deposits and active layer permafrost
 1201 (Tesi et al., 2014). ESS is short for the East Siberian Shelf.